Journal of Experimental Psychology:
Human Perception and Performance
2003, Vol. 29, No. 2, 343–362

0096-1523/03/$12.00 DOI: 10.1037/0096-1523.29.2.343

Behavioral Dynamics of Steering, Obstacle Avoidance, and Route Selection

Brett R. Fajen and William H. Warren
Brown University

The authors investigated the dynamics of steering and obstacle avoidance, with the aim of predicting routes through complex scenes. Participants walked in a virtual environment toward a goal (Experiment 1) and around an obstacle (Experiment 2) whose initial angle and distance varied. Goals and obstacles behave as attractors and repellers of heading, respectively, whose strengths depend on distance. The observed behavior was modeled as a dynamical system in which angular acceleration is a function of goal and obstacle angle and distance. By linearly combining terms for goals and obstacles, one could predict whether participants adopt a route to the left or right of an obstacle to reach a goal (Experiment 3). Route selection may emerge from on-line steering dynamics, making explicit path planning unnecessary.

How do humans and other animals locomote effortlessly through a complex environment, steering toward goals, avoiding obstacles, and adopting particular routes through the cluttered landscape? This basic problem has inspired a good deal of research on the optical information available to a moving observer and the visual perception of self-motion (Gibson, 1958/1998; Land, 1998; Lee, 1980; Warren, in press). At the same time, research on motor coordination has demonstrated that the action system generates stable movement patterns and qualitative transitions that can be characterized using concepts from nonlinear dynamics (Kelso, 1995; Kugler & Turvey, 1987), including stable gaits and gait transitions (Collins & Stewart, 1993; Diedrich & Warren, 1995; Jeka, Kelso, & Kiemel, 1993; Kay & Warren, 2001; Schöner, Jiang, & Kelso, 1990). To date, however, most research on coordination dynamics has focused on fairly simple tasks such as stationary rhythmic movement or bimanual coordination. To develop an account of more complex, adaptive behavior that depends on interactions with the environment, we believe it is necessary to integrate information-based and dynamical approaches. In the present article, we attempt such an account of visually controlled locomotion. Specifically, we derive a dynamical model of steering and obstacle avoidance from empirical observations of human walking and use it to predict routes through a simple scene. (For background on dynamical systems, see Strogatz, 1994; for applications to behavior, see Kelso, 1995, and Schöner, Dose, & Engels, 1995.)

The dynamics of perception and action (Warren, 1998, 2002) can be described at two levels of analysis. The first level characterizes the interaction between an agent and its environment. Specifically, the actions of the agent affect its relation to the environment and make new information available, according to what Gibson (1979) called *laws of ecological optics.* Reciprocally, this information is used to regulate action, according to what Warren (1988) called *laws of control.* The problem at this level is to identify the informational variables that are used to guide behavior and to formalize the control laws by which they regulate action. Researchers are just beginning to investigate the information and control laws for locomotion (Duchon & Warren, 2002; Fajen, 2001; Rushton, Harris, Lloyd, & Wann, 1998; Warren, Kay, Zosh, Duchon, & Sahuc, 2001).

When an agent interacts with a structured environment over time, observed patterns of behavior emerge. The second level of analysis characterizes the temporal evolution of this behavior, which we call the *behavioral dynamics.* Briefly, goal-directed behavior can often be described by changes in a few *behavioral variables.* Observed behavior corresponds to trajectories in the state space of behavioral variables, and it may be formally expressed in terms of solutions to a system of differential equations. Goals correspond to *attractors* or regions in state space toward which trajectories converge. Conversely, states to be avoided correspond to *repellers,* regions from which trajectories diverge. Sudden changes in the number or type of these fixed points are known as *bifurcations,* which correspond to qualitative transitions in behavior. Thus, the problem at the second level of analysis is to identify a system of differential equations (i.e., a dynamical system) whose solutions capture the observed behavior. Here we seek to do precisely this for the behavioral dynamics of steering and obstacle avoidance.

These two levels of analysis are linked because the behavioral outcome at the second level is a consequence of control laws interacting with the biomechanics of the body and physics of the environment at the first level. Thus, the nervous system cannot simply prescribe behavior; it must adopt control laws that give rise to attractors and repellers in the behavioral dynamics corresponding to the intended behavior. A model of the behavioral dynamics may allow us to draw some inferences about the form of control laws, a question to which we return in the General Discussion.

Brett R. Fajen and William H. Warren, Department of Cognitive and Linguistic Sciences, Brown University.

This research was supported by National Eye Institute Grant EY10923, National Institute of Mental Health Grant K02 MH01353, and National Science Foundation Grant NSF 9720327. We thank Bruce Kay and Philip Fink for their assistance with the analyses and modeling and Gregor Schöner for helpful discussions.

Correspondence concerning this article should be addressed to Brett R. Fajen, who is now at the Department of Cognitive Science, Carnegie Building 305, Rensselaer Polytechnic Institute, 110 Eighth Street, Troy, New York 12180. E-mail: fajenb@rpi.edu

Toward a Dynamical Model of Steering and Obstacle Avoidance

Our aim in this article is to apply this dynamical framework to the basic locomotor behavior of steering toward a goal and avoiding an obstacle. A similar analysis of steering toward targets (attractors) was performed by Reichardt and Poggio (1976) in the housefly, although they did not consider the contribution of obstacles (repellers). We are indebted to the approach of Schöner and Dose (1992; Schöner et al., 1995), who developed a dynamical control system for mobile robots that demonstrated the role of repellers in steering control. Here we model observed behavior at the second level of the behavioral dynamics.[1] Our procedure is (a) to identify a set of behavioral variables for steering and obstacle avoidance and introduce the general form of the model, (b) to measure these behavioral variables for human walking, (c) to develop a fully specified model of the behavioral dynamics, and (d) to attempt to predict routes in simple scenes by linearly combining terms for goals and obstacles.

Consider an agent moving in a simple environment at a constant speed s and a heading direction ϕ, defined with respect to a fixed exocentric reference axis (see Figure 1A).[2] From the agent's current position (x, z), a goal lies in the direction ψ_g at a distance d_g, and an obstacle lies in the direction ψ_o at a distance d_o. To steer to the goal, the agent must change its direction of locomotion with a turning rate $\dot{\phi}$ until it is heading toward the goal, such that the heading error $\phi - \psi_g = 0$ and $\dot{\phi} = 0$. At the same time, the agent must turn away from the obstacle, such that $\phi - \psi_o \neq 0$ when $\dot{\phi} = 0$. Because ϕ and $\dot{\phi}$ describe the current behavioral state, we adopt them as behavioral variables.

From the agent's point of view, the positions of goals and obstacles can also be represented in egocentric coordinates (Figure 1B). For example, the direction of the goal with respect to the heading (the *goal angle*) is equal to $\phi - \psi_g$, and the direction of an obstacle with respect to the heading (the *obstacle angle*) is equal to $\phi - \psi_o$. These angles are visually available to the agent, and there is evidence that both the object-relative heading specified by optic flow and the egocentric direction of a goal with respect to the locomotor axis contribute to the visual control of locomotion (Li & Warren, 2002; Rushton et al., 1998; Warren et al., 2001).

A dynamical model of steering and obstacle avoidance consists of a system of differential equations with attractors and repellers that correspond to goals and obstacles. To develop the reader's intuition of the formal techniques of dynamics, we begin by illustrating simple first-order dynamical systems that contain attractors and repellers. We then build on these equations to develop a higher order system that more closely characterizes the behavioral dynamics of steering and obstacle avoidance in humans.

The simplest description of the steering dynamics is that heading is stabilized in the direction of the goal at ψ_g. Following Schöner et al. (1995), we can represent this as a first-order system by a function that specifies the turning rate for each possible value of heading. For example, the dynamics of steering toward a goal involve turning toward the goal at ψ_g at a rate that increases as heading increases away from the goal. This might be expressed as a linear relationship between goal angle $(\phi - \psi_g)$ and turning rate $(\dot{\phi})$, represented as a line that intersects the abscissa at $\phi - \psi_g = 0$ with a negative slope (see Figure 2A):

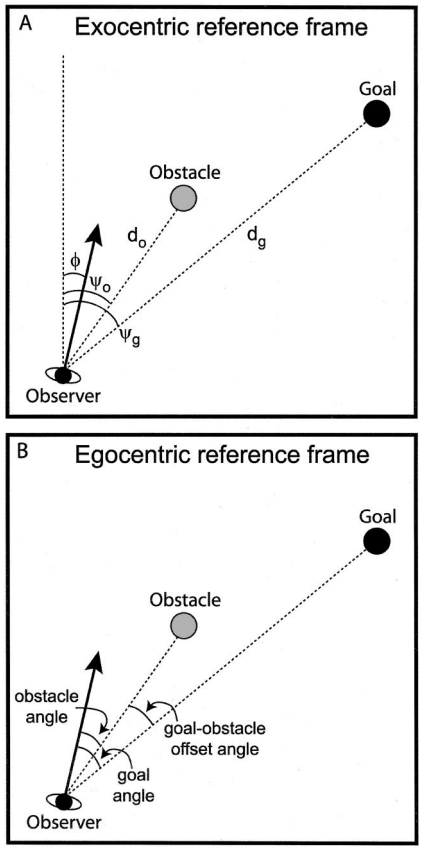

Figure 1. Plan view of an observer moving through an environment containing a goal and an obstacle. A: The vertical dotted line is a fixed, exocentric reference line used to define the observer's direction of locomotion (ϕ), the direction of the goal (ψ_g), and the direction of the obstacle (ψ_o); d_g and d_o correspond to the distance from the observer to the goal and obstacle, respectively. B: The goal and obstacle angles are defined in an egocentric reference frame with respect to the observer's direction of locomotion.

$$\dot{\phi} = -k_g(\phi - \psi_g). \quad (1)$$

Headings to the right of ψ_g thus yield a negative turning rate (to the left), and headings to the left of ψ_g yield a positive turning rate (to the right). Thus, the point $\phi - \psi_g = 0$ serves as an *attractor*, such that as one turns toward the goal the turning rate goes to zero. The slope k_g determines the goal's "attractiveness," that is, the relaxation time to the attractor as well as its stability.

[1] Schöner et al. (1995) used the term *behavioral dynamics* to refer to a robot control algorithm independent of its physical implementation, whereas we develop the concept as a description of the observed behavior of a physical system. In our view, stable behavior is achieved within given physical and biomechanical constraints, and thus the behavioral dynamics are a consequence of control laws acting in a physical system.

[2] The advantage of a fixed exocentric reference axis is that turning rate is measured with respect to the world, goals and obstacles can be represented as specific values of the behavioral variables independent of the current heading, and steering can be represented by trajectories through the state space of behavioral variables.

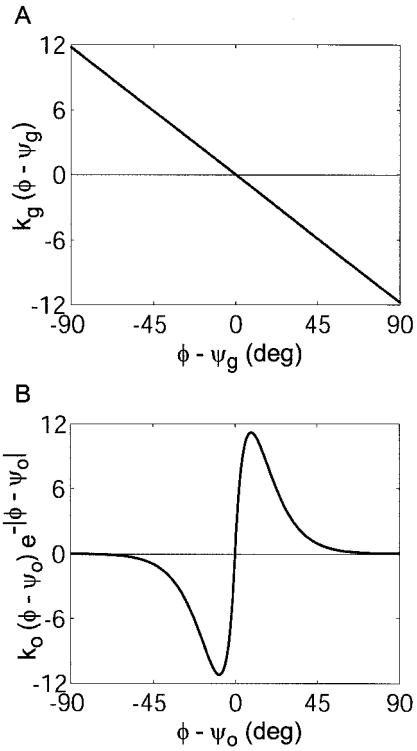

Figure 2. Plots of steering and obstacle avoidance terms. A: Steering term as a function of goal angle. B: Obstacle avoidance term as a function of obstacle angle.

Conversely, the dynamics of obstacle avoidance involve turning away from an obstacle at ψ_o at a decreasing rate. We might represent this by multiplying obstacle angle ($\phi - \psi_o$) by an exponential function, so that the curve intersects the abscissa at $\phi - \psi_o = 0$ with a positive slope (Figure 2B):

$$\dot{\phi} = k_o (\phi - \psi_o) e^{-|\phi - \psi_o|}. \quad (2)$$

Headings to the right of ψ_o yield a positive turning rate (to the right) that asymptotes to zero as the agent turns away from the obstacle, and headings to the left of ψ_o yield a negative turning rate that also asymptotes to zero. The unstable fixed point $\phi - \psi_o = 0$ thus functions as a repeller, with its "repulsion" determined by the slope of the function through that point, specified by parameter k_o.

The dynamics of steering through complex environments might be captured by linearly combining such functions, one for each goal and obstacle, such that the net turning rate is determined by their sum at each value of heading:

$$\dot{\phi} = -k_g (\phi - \psi_g) + k_o (\phi - \psi_o) e^{-|\phi - \psi_o|}. \quad (3)$$

This is analogous to Reichardt and Poggio's (1976) superposition rule for targets in insect flight control, and it has the advantage that the complexity of the model scales linearly with the complexity of the environment. As the agent moves through the world, the angles of the goal (ψ_g) and obstacles (ψ_o) shift along the ϕ axis. The location of attractors and repellers determined by the total function also shifts, influencing the current heading at each point on the agent's path.

However, such a first-order description does not capture the fact that any physical body with inertia cannot make instantaneous changes in angular velocity. To characterize the dynamics of observed behavior, one requires at least a second-order system that maps values of heading (ϕ) and turning rate ($\dot{\phi}$) onto angular acceleration ($\ddot{\phi}$). An intuitive example of a second-order system is a mass-spring,

$$\ddot{x} = -\frac{b}{m}\dot{x} - \frac{k}{m}x, \quad (4)$$

where m is mass, b is the damping coefficient, and k is the stiffness of the spring. A fixed point in a two-dimensional system is defined as the position (x) at which both velocity ($\dot{x}$) and acceleration ($\ddot{x}$) equal zero. Setting $\dot{x}$ and $\ddot{x}$ equal to zero for the system described in Equation 4, it is clear that the fixed point is located at $(x, \dot{x}) = (0, 0)$. Similarly, a mass-spring system described by the equation

$$\ddot{x} = -\frac{b}{m}\dot{x} - \frac{k}{m}(x - p) \quad (5)$$

has a fixed point at $(x, \dot{x}) = (p, 0)$.

Substituting the angular variables ϕ, $\dot{\phi}$, and ψ_g for x, $\dot{x}$, and p, and replacing mass with the moment of inertia I, yields

$$\ddot{\phi} = -\frac{b}{I}\dot{\phi} - \frac{k_g}{I}(\phi - \psi_g). \quad (6)$$

This system contains an attractor at $(\phi, \dot{\phi}) = (\psi_g, 0)$. From here on we suppress the inertia term I and assume that the b and k parameters express the ratios of damping and stiffness to the body's moment of inertia, so that b has units of 1/s and k has units of $1/s^2$. We can add a saddle point creating repulsion away from $(\phi, \dot{\phi}) = (\psi_o, 0)$ as follows:

$$\ddot{\phi} = -b\dot{\phi} - k_g (\phi - \psi_g) + k_o (\phi - \psi_o) e^{-|\phi - \psi_o|}. \quad (7)$$

Steering toward a goal while avoiding an obstacle thus forms a trajectory through the space of behavioral variables (ϕ, $\dot{\phi}$) toward the goal at (ψ_g, 0) and away from the obstacle at (ψ_o, 0). At any point, the current heading direction is, in effect, the resultant of all "spring forces" acting on the agent at that position in the environment. The agent's turning rate ($\dot{\phi}$) is some function of the current goal and obstacle angles with respect to the heading direction. Reciprocally, the motion of the agent to a new (x, z) position in the environment alters these angles. Locomotion in an environment is thus a four-dimensional system, because to predict the agent's future position we need to know its current position (x, z), heading (ϕ), and turning rate ($\dot{\phi}$), assuming that speed is constant. (Full model equations appear in the Appendix.)

The actual shape of an observed trajectory for human walking depends on the manner in which people turn toward goals and away from obstacles. If angular acceleration ($\ddot{\phi}$) is influenced by additional factors such as the distances of goals and obstacles, then $\ddot{\phi}$ for a given heading and turning rate also depends on these variables. We thus designed a series of experiments intended to measure how the angle and distance to goals and obstacles influence angular acceleration. These observations were then used to specify a dynamical model in which the particular forms of goal

and obstacle components were chosen to reflect the empirical observations. We thus sought to construct a model that captured the basic characteristics of human steering and obstacle avoidance.

Our aim was to use the model to predict route selection in a simple scene, when an agent must choose to detour left or right around an obstacle to reach a goal. Because the model determines turning from occurrent information about goals and obstacles, the route emerges from the local steering dynamics, rather than being planned in advance. This contrasts with a common approach in robotics, in which a route is explicitly planned on the basis of an internal world model. Our results demonstrate that it is possible to account for route selection as a consequence of elementary on-line behaviors for steering and obstacle avoidance.

General Method

Apparatus

The experiments were conducted in the Virtual Environment Navigation Laboratory (VENLab) at Brown University. Participants walked freely in a 12 m × 12 m room while viewing a virtual environment through a head-mounted display (HMD; Proview 80, Kaiser Electro-optics, Inc., Carlsbad, CA). The HMD provided stereoscopic viewing with a 60° (horizontal) × 40° (vertical) field of view and a resolution of 640 × 480 pixels. A black isolation shield was placed over the HMD, so the surrounding field was dark.

The participant's head position (4 mm root-mean-square error) and orientation (0.1° root-mean-square error) were measured by a hybrid inertial–ultrasonic tracking system (IS-900, Intersense, Burlington, MA) with six degrees of freedom, at a sampling rate of 60 Hz. Displays were generated on an SGI Onyx 2 Infinite Reality workstation (Silicon Graphics, Inc., Mountain View, CA) at a frame rate of 60 Hz, using WorldToolKit software (Sense8, Inc., San Rafael, CA). Head coordinates from the tracker were used to update the display with a latency of approximately 50 ms (three frames).

Displays

The virtual environment consisted of a ground plane (50 m^2) mapped with a random noise texture of black and white squares and a black sky (see Figure 3). Before each trial, two cylindrical red markers appeared on the ground plane. Participants stood on one marker and faced the other. The start of a trial was signaled by the marker color changing to green, whereupon the participant began walking in the direction of the distant marker. Depending on the experiment, a goal or an obstacle (or both) subsequently appeared on the ground. Goal posts were blue or green granite-textured cylinders standing on end, 2.475 m (1.5 eye heights) tall with a radius of 0.1 m; obstacles were red or blue granite-textured cylinders, 1.98 m (1.2 eye heights) tall, with a radius of 0.1 m. The participant's task was to walk to the goal. When the participant reached the goal post, it disappeared with a "popping" noise and the red markers reappeared on the ground in their previous locations. Participants walked to the marker in front of them and turned around to face the other one, in preparation for the next trial.

Procedure

Prior to the experiment, the lens separation in the HMD was adjusted to each participant's interocular distance. To ensure that the participant could fuse a stereo image pair, a random-dot stereogram of a rectangle was presented and, if necessary, the lenses were adjusted further until the rectangle was visible.

Each participant completed approximately two to four practice trials, until they demonstrated that they understood the task and could walk comfortably through the virtual environment while wearing the HMD. The experiment began immediately after the practice trials. Participants were prompted to take a break and remove the HMD approximately halfway through the experiment. They were also informed that they could take breaks between trials or stop entirely if they experienced symptoms of simulator sickness. Only one participant (in Experiment 3) reported such symptoms and discontinued the experiment.

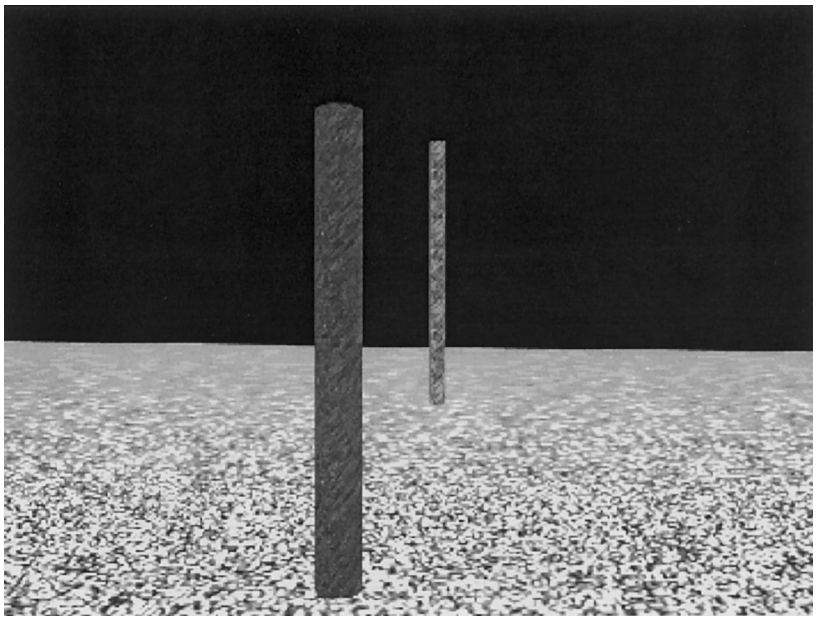

Figure 3. Sample frame from virtual environment showing goal post (light cylinder) and obstacle post (dark cylinder) resting on a textured ground plane.

Data Analysis

The x- and z-coordinates of head position were recorded by computer on every other frame (sampling rate of 30 Hz). Both the x and z time series were filtered using a forward and backward 4th-order lowpass Butterworth filter with a cutoff frequency of 0.6 Hz, to reduce the effects of gait oscillations. The filtered position data were used to compute the participant's direction of motion (the heading ϕ) in exocentric coordinates in each frame according to the following equation:

$$\phi_i = \tan^{-1}\left(\frac{x_i - x_{i-1}}{z_i - z_{i-1}}\right), \quad (8)$$

where x_i and z_i are the head position coordinates on the ith frame. Turning rate ($\dot{\phi}$) in deg/s was computed by multiplying the difference in motion direction (ϕ) on adjacent frames by 30, the number of frames recorded per second. The angle of the goal (ψ_g) and obstacle (ψ_o) with respect to the reference axis in each frame were computed from the following equations:

$$\psi_g = \tan^{-1}\left(\frac{X_g - x}{Z_g - z}\right) \quad (9)$$

and

$$\psi_o = \tan^{-1}\left(\frac{X_o - x}{Z_o - z}\right), \quad (10)$$

where X and Z are the goal or obstacle coordinates.

Mean paths in each condition were computed as follows. In each frame, the value of the x-coordinate was binned in intervals of 0.1 m along the z-axis. The contents of each bin were then averaged over all trials in a condition for each participant, to determine the mean x-coordinate for each z-axis interval. Mean paths in each condition were then averaged over participants. To normalize across different initial headings, we also computed the goal angle with respect to heading as $\phi - \psi_g$ and obstacle angle as $\phi - \psi_o$. Mean time series of goal and obstacle angle for each condition were computed by averaging their values at each time step across all trials and then across all participants.

Experiment 1: Steering to a Goal

The first experiment was designed to investigate steering toward a goal, specifically how the turning rate depends on goal angle and distance. Participants began each trial by walking in a specified direction. Subsequently, a goal object appeared and participants simply walked to the goal. In Experiment 1a, we varied the initial angle of the goal with respect to the direction of heading ($\phi - \psi_g$) while holding initial goal distance (d_g) fixed. In Experiment 1b, initial goal angle was crossed with initial goal distance, to assess their interaction. The purpose of these experiments was to collect descriptive data in order to develop a model of the behavioral dynamics.

Method

Participants. Eight undergraduate and graduate students, 4 women and 4 men who ranged in age from 18 to 28 years, participated in Experiment 1a. Ten other students, 6 women and 4 men who ranged in age from 18 to 36 years, participated in Experiment 1b. None reported any visual or motor impairment. They were paid $6 for their participation.

Displays. At the beginning of each trial, the participant stood on one red marker, faced the other, and started walking when the markers turned green. After traveling 0.5 m, the markers disappeared and participants were instructed to continue walking and looking in the same direction. After traveling another 0.5 m, a blue goal post appeared off to one side. In Experiment 1a, the goal appeared at an angle of ±5°, 10°, 15°, 20°, or 25° to the right (+) or left (−) of the direction of travel, at a distance of 4 m. In Experiment 1b, the goal appeared at an angle of ±10° or 20° and a distance of 2, 4, or 8 m.

Design. Experiment 1a had a 5 (goal angle) × 2 (left, right) factorial design with eight trials per condition, for a total of 80 trials. Experiment 1b had a 2 (goal angle) × 2 (left, right) × 3 (goal distance) design with eight trials per condition, a total of 96 trials. All variables were within-subject, and trials were presented in a random order.

Results and Discussion

Experiment 1a. Mean paths for each initial goal angle are presented in Figure 4A, plotted so that the participant is at location (0, 0) when the goal post appears. The paths reveal that participants began turning toward the goal about 0.5 m after it appeared, and they turned at faster rates with larger initial goal angles. They completed the turn well before reaching the goal and followed an approximately linear path for the remainder of the approach. The mean time series of goal angle (Figure 5A) also illustrates the influence of initial goal angle on angular acceleration and turning rate. For larger initial goal angles (y-axis), the curves exhibit

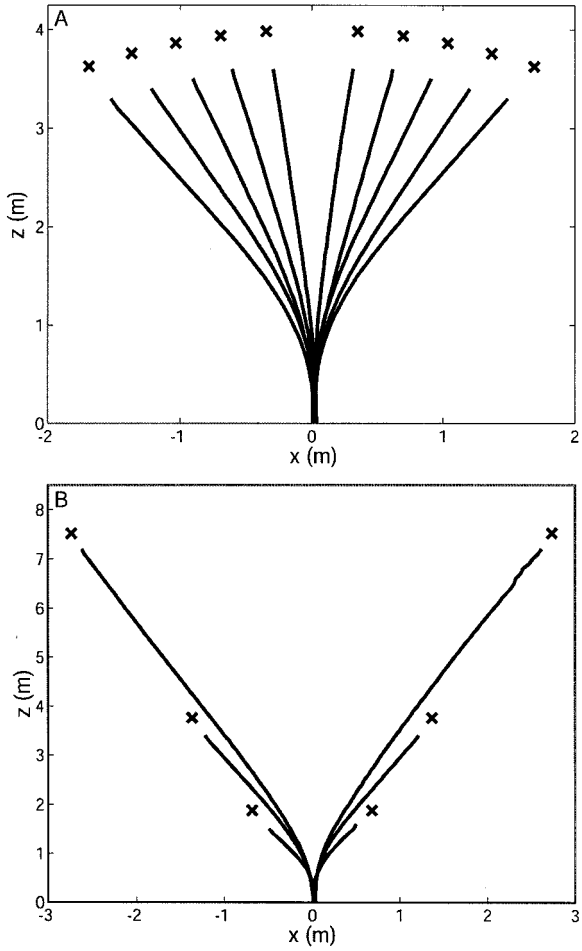

Figure 4. Mean paths to goals. A: At ±5°, 10°, 15°, 20°, and 25° in Experiment 1a. B: At 2, 4, and 8 m in the ±20° condition of Experiment 1b.

steeper slopes, corresponding to greater angular acceleration and faster turning rates, with the consequence that all curves converge onto zero at approximately the same time. The small error bars, corresponding to ±1 standard deviation of the mean subject data, show that behavior was consistent across participants. Although individuals differed slightly in terms of the rate at which they turned toward the goal, such differences were minor and can be captured in terms of small variations in model parameters. Figure 6 presents the goal angle time series for eight trials from one participant in the 25° condition, illustrating that behavior was quite consistent from trial to trial for individual participants as well.

For convenience, we plotted mean trajectories for all participants in the modified state space of goal angle and turning rate ($\phi - \psi_g$, $\dot{\phi}$) in Figure 7A.[3] Plotting the goal angle rather than the absolute heading simply puts the goal at the origin, normalizing trajectories for different initial conditions by aligning them on a common goal state. Given initial conditions on the *x*-axis of a specified goal angle and a zero turning rate, participants rapidly accelerated to a peak turning rate and then more gradually decelerated to a stop at ($\phi - \psi_g$, $\dot{\phi}$) = (0, 0). Steering to a goal thus exhibits the expected point attractor dynamics, but with more complicated trajectories than those of Equation 1. Note that the height of the peak for each curve increases with initial goal angle, confirming that participants accelerated more rapidly to higher turning rates with larger initial angles. The main effect of initial goal angle on maximum turning rate (maximum $\dot{\phi}$) was significant, $F(4, 28) = 139.74$, $p < .01$ (see Table 1). Thus, Experiment 1a revealed that angular acceleration and maximum turning rate toward a goal increase with goal angle.

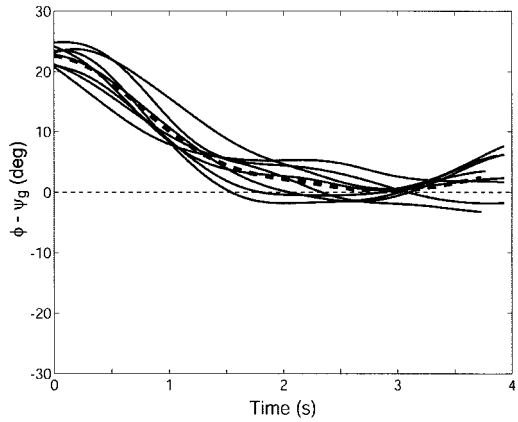

Figure 6. Sample goal angle time series for 1 participant in the 25° condition of Experiment 1a. Solid lines are individual trials and the dotted line is the mean time series for that participant in the 25° condition.

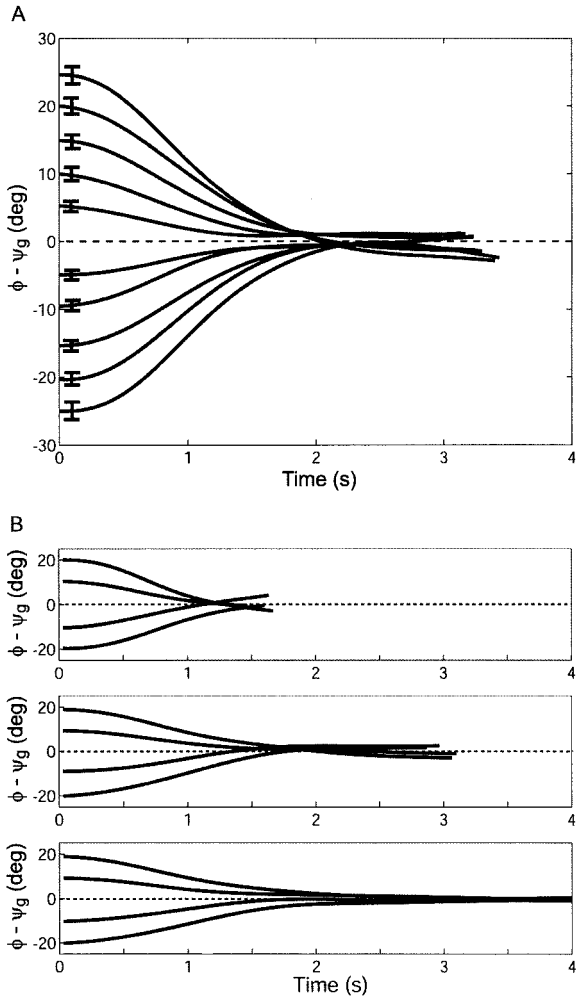

Figure 5. Mean goal angle time series. A: In the ±5°, 10°, 15°, 20°, and 25° conditions of Experiment 1a. B: In the 2-, 4-, and 8-m conditions of Experiment 1b. Error bars in A correspond to ±1 standard deviation of the mean participant data.

We also analyzed walking speed to determine whether participants changed speed during the trial. Walking speed was fairly constant during the central portion of the trial, with a similar pattern exhibited by all participants across all conditions. Walking speed increased from 0 m/s to a mean of 1.01 m/s ($SD = 0.06$) during the first meter of walking, at which point the goal appeared. Walking speed continued to increase gradually to a mean maximum of 1.16 m/s ($SD = 0.08$). It then remained roughly constant until about a second before the participant reached the goal, at which point it dropped sharply to 0.11 m/s ($SD = 0.01$) at contact. Maximum walking speed decreased very slightly as initial goal angle increased (1.19, 1.17, 1.16, 1.16, and 1.13 m/s for 5°, 10°, 15°, 20°, and 25°, respectively).

Experiment 1b. Mean paths for each initial goal distance in the 20° goal angle condition are shown in Figure 4B (mean paths in the 10° condition were qualitatively similar). In all initial goal distance conditions, participants completed (or nearly completed) their turn before reaching the goal, and they appeared to turn faster toward nearer goals. This is confirmed by the mean goal angle time series (Figure 5B), in which the curves converge onto zero earlier when the goal is closer, with a concomitant increase in slope. Figure 7B depicts mean trajectories in state space for the three

[3] Note that these are not actually phase portraits of a fixed dynamical system, because as the observer travels forward through the environment the angle ψ continually changes. Thus, the location of the attractor in the ϕ dimension and hence the dynamical system also evolve over the course of a trial.

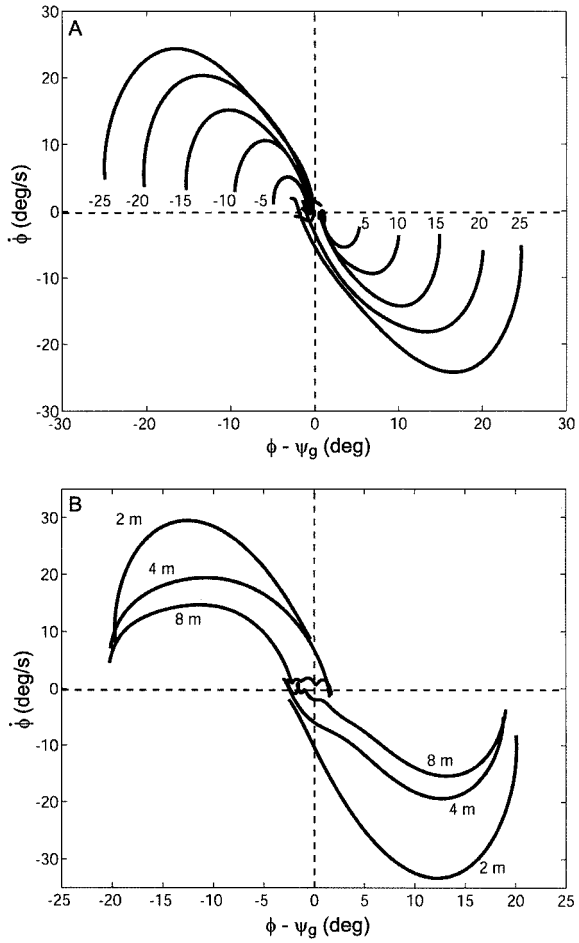

Figure 7. Trajectories in the state space of turning rate ($\dot{\phi}$) by goal angle ($\phi - \psi_g$). A: At ±5°, 10°, 15°, 20°, and 25° in the 4-m condition of Experiment 1a. B: At 2, 4, and 8 m in the 20° condition of Experiment 1b.

initial goal distances in the 20° goal angle condition. A similar pattern of acceleration and deceleration with point attractor dynamics occurs at each distance, with larger peak turning rates for closer goals. The analysis of maximum turning rate revealed significant main effects of initial goal angle, $F(1, 9) = 303.6$, $p < .01$, and initial goal distance, $F(2, 18) = 46.01$, $p < .01$, as well as a significant interaction, $F(2, 18) = 20.71$, $p < .01$ (see Table 1). The effect of goal distance indicates that participants accelerated more rapidly toward nearby goals, and the interaction indicates that this effect is greater at larger goal angles. Thus, Experiment 1b indicates that angular acceleration and turning rate increase with initial goal angle but decrease with initial goal distance.

As in Experiment 1a, walking speed was fairly constant during most of the trial. Walking speed increased from 0 m/s to a mean of 0.98 m/s ($SD = 0.9$) in the first meter, and then it increased gradually to a mean maximum of 1.14 m/s ($SD = 0.10$) before dropping to 0.10 m/s ($SD = 0.01$) in the last second before contact. Maximum walking speed decreased slightly as initial goal angle increased (1.15 and 1.13 m/s for 10° and 20°, respectively) and increased with initial goal distance (1.07, 1.18, and 1.19 m/s for 2, 4, and 8 m, respectively). Thus, walking speed was roughly constant throughout the portion of the trial during which participants were turning. For the sake of simplicity, we ignored these minor variations in our simulations and assumed that participants maintained a constant walking speed.

The purpose of Experiment 1 was to determine how initial goal angle and distance influence turning toward a goal. The results demonstrate that angular acceleration increases with goal angle and decreases with goal distance. These observations are consistent with the task of efficiently steering toward a goal. If angular acceleration were unaffected by initial goal distance and angle, an observer might not turn fast enough to hit a nearby goal or to reach a goal at a large angle, thereby passing to the outside of the goal. Conversely, the observer might generate unnecessary torque to accelerate toward a distant goal or one at a small angle. Thus, the dependence of angular acceleration on goal angle and distance guarantees effective steering over a wide range of initial conditions.

Goal component of the model. Based on these results, we derived a model of the behavioral dynamics of steering toward a goal. The pattern of acceleration and deceleration evident in the state space trajectories confirmed that at least a second-order system was required. Moreover, the dependence of turning rate on goal distance added another variable. The following model thus has the form of Equation 6, with angular acceleration $\ddot{\phi}$ a function of both goal angle ($\phi - \psi_g$) and goal distance (d_g):

Table 1
Maximum Turning Rates ($\dot{\phi}$) in Experiments 1 and 2

Condition	Maximum turning rate (deg/s)	
	M	*SD*
Experiment 1a		
Initial goal angle (deg)*		
5	9.48	2.30
10	13.11	2.38
15	17.94	2.77
20	22.17	2.98
25	27.12	4.38
Experiment 1b		
Initial goal angle (deg)*		
10	16.20	3.06
20	25.83	3.69
Initial goal distance (m)*		
2	28.35	6.25
4	18.73	2.41
8	15.97	2.37
Experiment 2		
Initial obstacle angle (deg)*		
1	15.69	4.03
2	15.18	3.10
4	13.17	3.40
8	10.74	3.39
Initial obstacle distance (m)*		
3	16.96	3.80
4	12.86	2.94
5	11.27	3.42

* $p < .001$.

$$\ddot{\phi} = -b\dot{\phi} - k_g(\phi - \psi_g)(e^{-c_1 d_g} + c_2), \quad (11)$$

where b, k_g, c_1, and c_2 are parameters. The "damping" term $-b\dot{\phi}$ acts as a frictional force that opposes angular motion. Damping is independent of heading (ϕ) and increases monotonically with turning rate ($\dot{\phi}$). Hence, we assume that it is proportional to turning rate. The "stiffness" term $k_g(\phi - \psi_g)$ reflects the finding from Experiment 1a that the angular acceleration toward a goal increases with goal angle. We provisionally assume that this function is linear (see Figure 2A), at least over the range of angles from −60° to 60°.[4] The "stiffness" parameter k_g determines the slope of the function and hence the attraction of the goal. Finally, the results of Experiment 1b are captured by the distance term $(e^{-c_1 d_g} + c_2)$, such that acceleration decreases exponentially with goal distance. This acts to modulate the parameter k_g, so that the slope of Figure 2A, and hence the attraction of the goal, decays with distance. The constant c_1 determines the rate of decay with distance and has units of 1/m, and c_2 scales the minimum acceleration so that it never goes to zero, even at large goal distances, and is dimensionless.

We simulated the model under the conditions tested in Experiment 1b to identify a single set of parameter values that best fit the mean time series of goal angle, using a least squares procedure. The best mean fit ($r^2 = .982$) was found with the parameter values $b = 3.25$, $k_g = 7.50$, $c_1 = 0.40$, and $c_2 = 0.40$. The simulation results appear in Figure 8B. Using the same parameter settings, we simulated the model under the conditions used in Experiment 1a and obtained a similar mean fit between the simulated and observed goal angle time series of $r^2 = .979$ (see Figure 8A). Note that the model exhibits the slight overshooting of $\phi - \psi_g = 0$ that is evident in the human data (compare Figures 5 and 8), a sign that the system is slightly underdamped.

More important, the model exhibited the two basic characteristics displayed by human participants. The state space trajectories for the model appear in Figure 9A, which depicts turning rate ($\dot{\phi}$) as a function of goal angle under the conditions tested in Experiment 1a. The trajectories show the same rapid acceleration to a peak turning rate, followed by a more gradual deceleration to a point attractor at (0, 0), as in the human data (compare Figure 7A). Moreover, the peak turning rate increases with initial goal angle in the same manner. The model trajectories for the conditions of Experiment 1b (see Figure 9B) also display a similar dependence on initial goal distance as the human data (compare Figure 7B). Thus, the model produces both a good quantitative and qualitative fit to the human behavior of steering toward a goal observed in Experiment 1.

Experiment 2: Avoiding an Obstacle

We designed Experiment 2 to investigate obstacle avoidance, specifically how turning away from an obstacle is influenced by obstacle angle and distance. Participants began each trial by walking in the direction of a goal. Subsequently, an obstacle appeared near their path, prompting them to detour around it on their way to the goal. We parametrically varied the initial angle of the obstacle with respect to the direction of heading ($\phi - \psi_o$) and the initial distance of the obstacle (d_g), and we recorded the behavioral variables. The purpose of the experiment was to collect descriptive data in order to develop an obstacle component for the model.

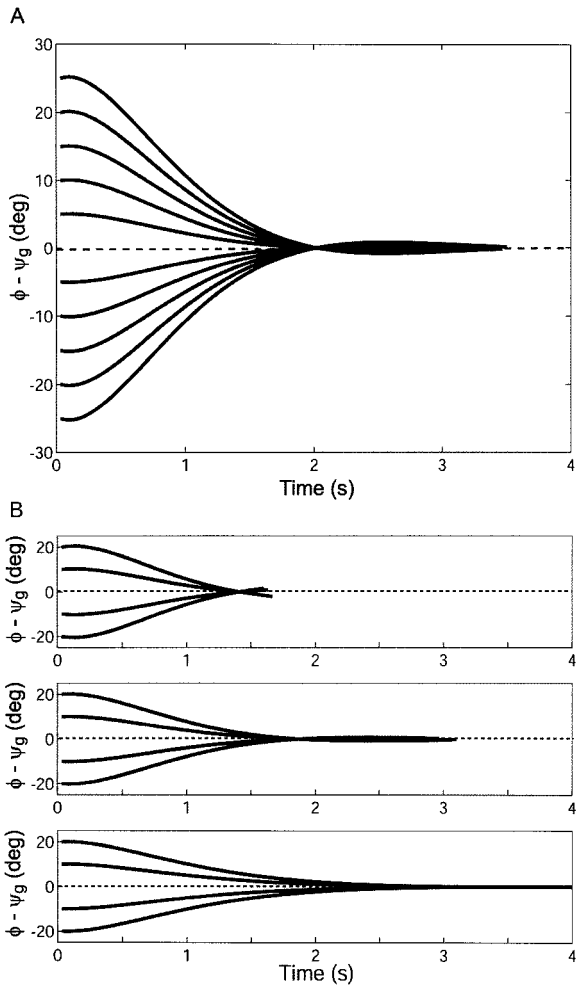

Figure 8. Simulated goal angle time series. A: In the ±5°, 10°, 15°, 20°, and 25° conditions of Experiment 1a. B: In the 2-, 4-, and 8-m conditions of Experiment 1b.

Method

Participants. Ten undergraduate and graduate students, 6 women and 4 men who ranged in age from 19 to 32 years, participated in Experiment 2. None reported having any visual or motor impairment. They were paid $6 for their participation.

Stimuli. As before, participants began walking when the distant marker turned green. However, in this experiment the green marker served as the goal and remained visible throughout the trial. After walking 1.0 m, a blue obstacle appeared slightly to the left or right at an angle of ±1°, 2°, 4°, or 8° from the direction of walking and at a distance of 3, 4, or 5 m. Participants were instructed to walk to the goal while avoiding the obstacle along the way, and they were told that they could walk to either side of the obstacle.

[4] Note that, because goal angle is a circular variable, the two ends of this curve must meet at ±180°, and thus it is unlikely to be linear over the whole range. Schöner et al. (1995) approximated it as a sine function, whereas the empirical "attractiveness function" in the housefly is more exponential in form, with a nearly linear region over the central 60° (Reichardt & Poggio, 1976).

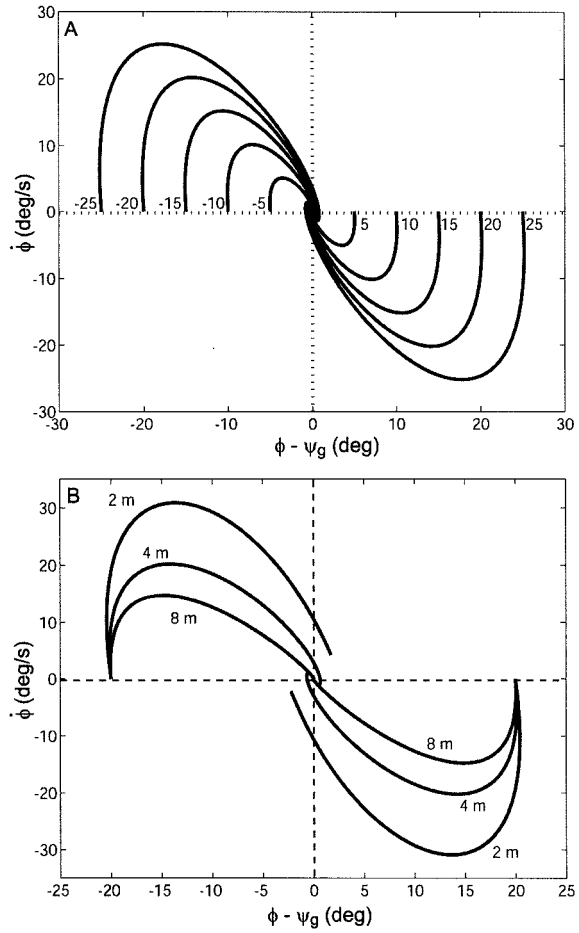

Figure 9. Simulated state space trajectories. A: At ±5°, 10°, 15°, 20°, and 25° in the 4-m condition of Experiment 1a. B: At 2, 4, and 8 m in the 20° condition of Experiment 1b.

To encourage detour behavior, a collision with the obstacle was signaled by a "ping" sound if the distance between the observation point and the center of the obstacle was less than 0.32 m. This value was determined from the radius of the obstacle (0.10 m) and the typical distance from the body midpoint to the shoulder (0.22 m; Warren & Whang, 1987). Participants were instructed to continue walking toward the goal if they collided with the obstacle, but to give the obstacle more room on future trials.

Design. The design for Experiment 2 was thus 4 (obstacle angle) × 2 (left, right) × 3 (obstacle distance), with all variables within-subject. There were four trials per condition, for a total of 96 trials, presented in a random order.

Results and Discussion

Effect of initial obstacle angle. Mean paths for the four obstacle angles in the 4 m distance condition appear in Figure 10A; the pattern at other distances is similar. Participants began turning away from the obstacle about 0.5 m after it appeared. Just before passing the obstacle, they began turning back toward the goal. The mean time series of obstacle angle in the same condition (Figure 11A) show that participants were repelled away from 0°, turning away from the obstacle such that the angle increases over time. The slopes of these curves also suggest that the angular acceleration away from the obstacle decreased with initial obstacle angle.

For convenience, we plotted mean trajectories in the state space of obstacle angle and turning rate ($\phi - \psi_o$, $\dot{\phi}$), putting the obstacle at the origin. This normalized the trajectories by aligning different initial conditions with respect to the repeller. Figure 12A depicts the state space trajectories for the four initial obstacle angles in the 4 m condition. This reveals repeller dynamics as the turning rate increases rapidly away from (0, 0) to a peak turning rate, then decreases again as participants pass the obstacle, and crosses zero as they begin to turn back in the opposite direction toward the goal. The peak turning rate decreased as initial obstacle angle increased, $F(3, 27) = 28.187$, $p < .01$, confirming that participants turned away from obstacles faster at smaller initial angles (see Table 1).

Effect of initial obstacle distance. Mean paths for each initial obstacle distance in the 4° angle condition appear in Figure 10B; the pattern is similar for the other angle conditions. Notice that the peak of the detour shifts with the *z*-position of the obstacle, as expected, but its amplitude also decreases slightly with obstacle distance. The time series of obstacle angle for each initial distance in this condition (Figure 11B) again diverge from 0°, but their slopes indicate faster turning rates for nearer obstacles. This is confirmed by the corresponding trajectories in Figure 12B. The peak turning rate decreased with obstacle distance, $F(2, 18) = 80.263$, $p < .01$ (see Table 1), indicating that participants turned away faster from nearer obstacles.

Walking speed was once again roughly constant during the trial, despite the presence of an obstacle. Mean walking speed increased from 0 to 1.00 m/s ($SD = 0.17$) in the first meter of travel, when

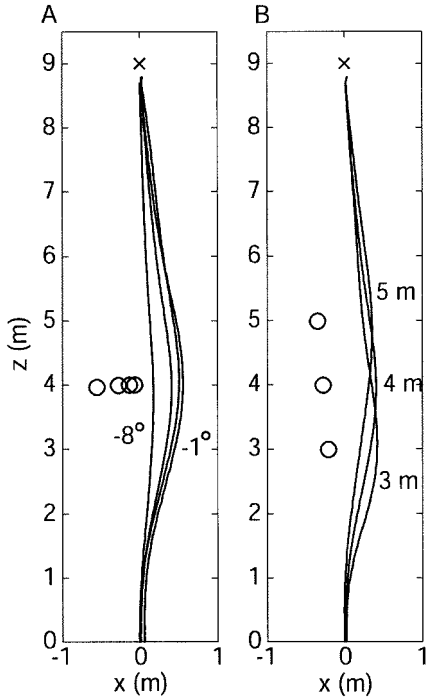

Figure 10. Mean paths around obstacles in Experiment 2. A: At −1°, −2°, −4°, and −8° in the 4-m condition. B: At 3, 4, and 5 m in the −4° condition.

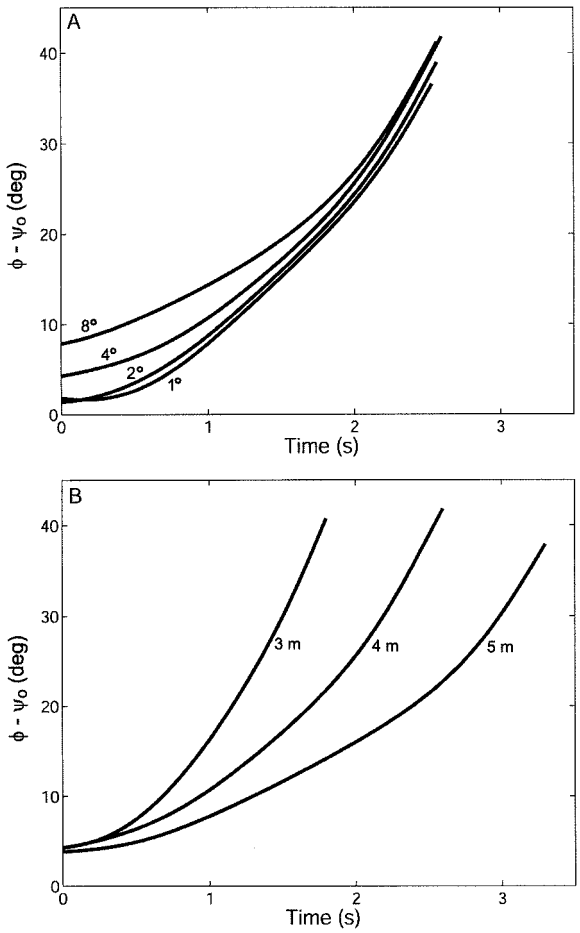

Figure 11. Mean obstacle angle time series in Experiment 2. A: At 1°, 2°, 4°, and 8° in the 4-m condition. B: At 3, 4, and 5 m in the 4° condition.

the obstacle appeared. Mean maximum walking speed was 1.21 m/s ($SD = 0.17$), which decreased to 0.08 m/s ($SD = 0.02$) in the last second before contact with the goal. Initial and final walking speed were unaffected by initial obstacle angle and distance. Maximum walking speed was unaffected by initial obstacle angle, but it increased slightly with initial obstacle distance (1.19, 1.21, and 1.23 m/s for 3, 4, and 5 m, respectively).

These results demonstrate that initial obstacle angle and distance influence turning away from an obstacle. The angular acceleration decreases with obstacle angle—it did not decrease with goal angle in Experiment 1—but it also decreases with obstacle distance, as it did with goal distance in Experiment 1. This is again consistent with efficient obstacle avoidance. If the angular acceleration were not affected by the obstacle angle and distance, then observers would risk colliding with nearby obstacles in their path, or they might generate unnecessary torque to avoid distant obstacles or those at large angles. Thus, having angular acceleration depend on obstacle angle and distance ensures effective obstacle avoidance under a variety of conditions.

We can summarize our findings thus far as follows: Angular acceleration increases with goal angle and decreases with goal distance, whereas it decreases with both obstacle angle and obstacle distance.

Obstacle component of the model. On the basis of the results of Experiment 2, we extended the model by adding an obstacle component:

$$\ddot{\phi} = -b\dot{\phi} - k_g(\phi - \psi_g)(e^{-c_1 d_g} + c_2) + k_o(\phi - \psi_o)(e^{-c_3|\phi - \psi_o|})(e^{-c_4 d_o}), \quad (12)$$

where k_o, c_3, and c_4 are obstacle parameters. First, the obstacle "stiffness" term $k_o(\phi - \psi_o)(e^{-c_1|\phi - \psi_o|})$ reflects the finding that the angular acceleration away from an obstacle decreases with obstacle angle. We modeled this with an exponential function that rises sharply from a heading of 0° to a peak close to the obstacle and then asymptotes to near zero (Figure 2B); the spread of this function is determined by parameter c_3, which has units of 1/rad. When heading to the right of an obstacle, this induces a positive acceleration away from the obstacle to the right; when heading to the left of the obstacle, the reflection of this function induces a negative acceleration to the left. Second, analogous to the goal component, the distance term ($e^{-c_4 d_o}$) reflects the finding that the turning rate away from an obstacle decreases exponentially with obstacle distance. It acts to modulate the parameter k_o, so that the

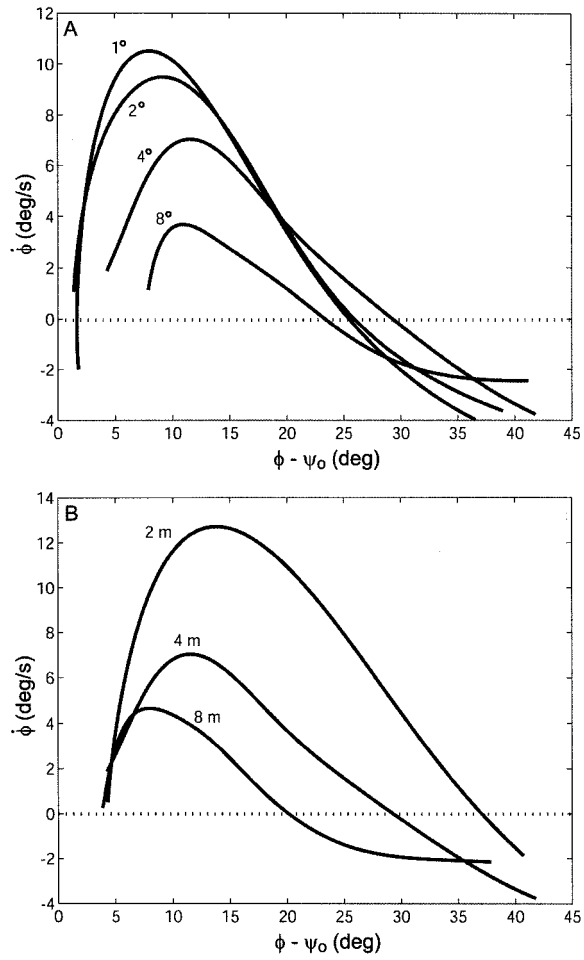

Figure 12. Trajectories in the state space of turning rate ($\dot{\phi}$) by obstacle angle ($\phi - \psi_o$) in Experiment 2. A: At 1°, 2°, 4°, and 8° in the 4-m condition. B: At 3, 4, and 5 m in the 4° condition.

amplitude of the function in Figure 2B, and hence the repulsion of the obstacle, decays with distance. Parameter c_4 determines the rate of decay with obstacle distance and has units of 1/m; in this case acceleration is allowed to asymptote to near zero as distance increases.

Using the parameter settings for b, k_g, c_1, and c_2 from Experiment 1, we simulated the extended model under the conditions of Experiment 2 to identify the values for k_o, c_3, and c_4 that best fit the mean obstacle angle time series, using a least-squares procedure. Only the portion of the obstacle angle time series before the observer passed the obstacle was used to evaluate the fit (i.e., before the observer's z-coordinate became greater than the obstacle's z-coordinate). The best mean fit ($r^2 = .975$) was found with values of $k_g = 198.0$, $c_3 = 6.5$, and $c_4 = 0.8$. Simulation results for the time series of obstacle angle appear in Figure 13, which illustrates that the model reproduces the effects of obstacle angle and distance observed in human behavior (compare Figure 11). Some curves are slightly less bowed, indicating that the model veers away from nearby obstacles sooner than human participants. Trajectories for the model demonstrate that the peak turning rate decreases with initial obstacle angle (Figure 14A) and with initial obstacle distance (Figure 14B). These trajectories are similar to those for participants in Figure 12, although the model reaches somewhat higher peak velocities. Nevertheless, the model successfully reproduces both key features of Experiment 2 and provides a good quantitative fit to the human data.

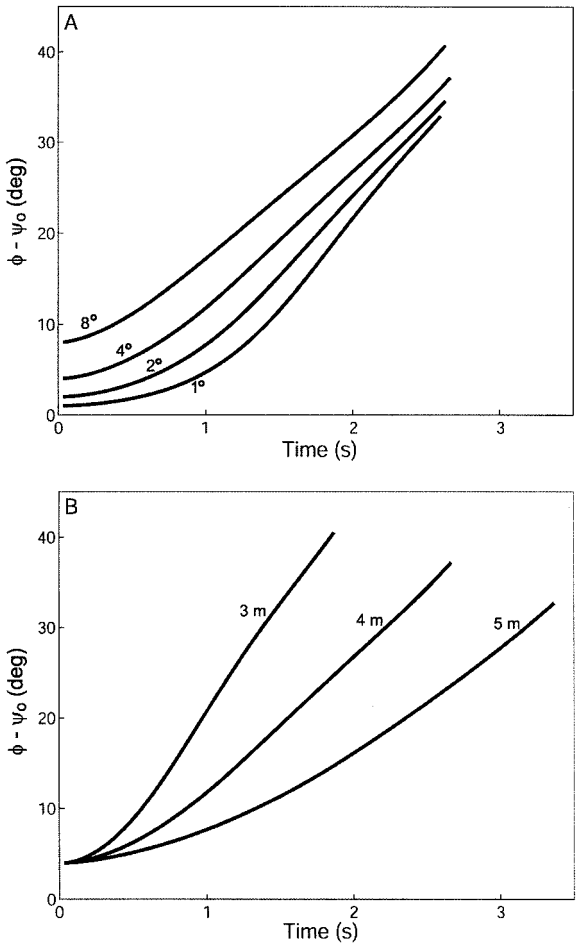

Figure 13. Simulated obstacle angle time series in Experiment 2. A: At 1°, 2°, 4°, and 8° in the 4-m condition. B: At 3, 4, and 5 m in the 4° condition.

Experiment 3: Route Selection With One Obstacle

Up to this point, we have only considered steering behavior with respect to a single goal or obstacle. In natural environments, however, configurations of objects often require observers to select a particular route to a goal from among different possible paths through an array of obstacles. The simplest case involves adopting one of two possible routes around an obstacle that lies between the observer's initial heading direction and the direction of the goal (see Figure 1). In this case, the observer could take either an outside (left) or an inside (right) path around the obstacle to reach the goal. What determines the actual route that the observer adopts?

A common approach to path planning is *model-based control*, which is characterized in robotics by a "sense-model-plan-act" scheme (Brooks, 1991; Moravec, 1981). Sensory information is used to construct an internal model of the environment, which represents the detailed 3-D layout of objects and surfaces in the scene. An action path is then explicitly planned on the basis of this model before being executed in the real world. For example, a path planning process might generate a route by determining the shortest distance to the goal or by following a minimum energy path through a landscape of potential "hills" corresponding to the locations of obstacles (Khatib, 1986).

An alternative approach, which Warren (1998) called *information-based control*, was anticipated by Gibson (1958/1998) and has been promoted in behavior-based robotics (Brooks, 1991; Duchon, Warren, & Kaelbling, 1998; Meyer & Wilson, 1991). In this case, available information is used to govern behavior in an on-line manner. The path adopted by the agent is not planned in advance; rather, it emerges as a consequence of the control laws by which information modulates action. Because occurrent information regulates control variables directly, an internal model of the environment and explicit path planning become unnecessary. What appears to be planned sequential behavior can thus emerge from the dynamic interaction between agent and environment, rather than implicating an action plan.

It is precisely this interaction that is captured in our model of the behavioral dynamics of steering and obstacle avoidance. The aim of Experiment 3 was to see whether the simplest case of human route selection could be accounted for by the model in terms of on-line steering dynamics, without recourse to explicit path planning. Note that this is not a critical test of the two approaches, but rather a demonstration of the sufficiency of a more parsimonious information-based approach.

In the present experiment, we recorded the routes taken by human participants around an obstacle to a goal, when the obstacle was located between the initial heading direction and the goal direction (Figure 1). We varied the initial distance of the goal (d_g) and the offset angle between the goal and the obstacle ($\psi_g - \psi_o$), to determine the conditions under which people switch from an outside to an inside path. We then tested whether the model predicted the observed routes, using the parameter values de-

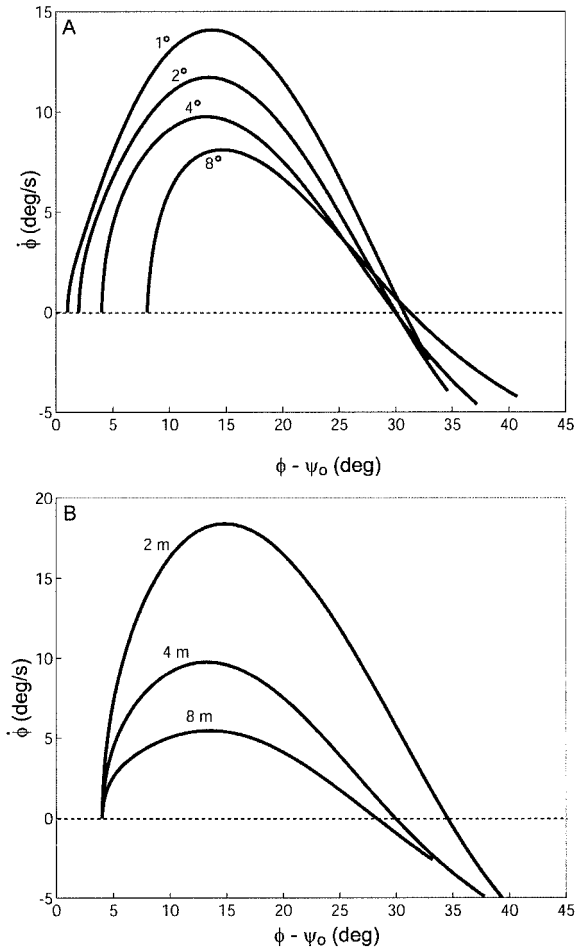

Figure 14. Simulated state space trajectories in Experiment 2. A: At 1°, 2°, 4°, and 8° in the 4-m condition. B: At 3, 4, and 5 m in the 4° condition.

rived in Experiments 1 and 2. To the extent that the model can reproduce the human paths, this would suggest that it is possible in principle to account for human route selection in terms of the dynamics of elementary behaviors for steering and obstacle avoidance.

Method

Participants. Ten undergraduate and graduate students, 4 women and 6 men who ranged in age from 18 to 26 years, participated in Experiment 3. None reported having any visual or motor impairment. They were paid $6 for their participation.

Stimuli. As in the previous experiments, participants began walking toward the distant marker when it turned green. After traveling 0.5 m, the markers disappeared and participants continued walking and looking in the same direction. After another 0.5 m, a blue goal post and a red obstacle appeared simultaneously on the left or right of the participant's path, with the obstacle in between the heading direction and the goal direction (refer to Figure 1A). First, we manipulated the initial offset angle between the obstacle and the goal ($\psi_g - \psi_o$ = 1°, 2°, 4°, or 8°) by holding the initial goal angle constant ($\phi - \psi_g$ = 15°) and varying the initial obstacle angle ($\phi - \psi_o$ = 14°, 13°, 11°, 7°). Second, we manipulated the initial goal distance (d_g = 5, 7, or 9 m) while holding the initial obstacle distance constant (d_o = 4 m). Participants were instructed to walk to the goal while avoiding the obstacle along the way, and they were told that they could pass to either side of the obstacle. As in Experiment 2, a collision with the obstacle was signaled by a "ping" if the point of observation came closer than 0.32 m to the center of the obstacle.

Design. The experiment had a 4 (offset angle) × 2 (left, right) × 3 (goal distance) factorial design, with all variables within-subject. There were four trials per condition, resulting in a total of 96 trials presented in a random order.

Results and Discussion

Mean paths for each initial offset angle (different panels) and initial goal distance (different curves) appear in Figure 15A, collapsed so all objects appear on the right of the initial heading. The most frequently selected route for each condition is represented by the solid curve. Participants took both inside and outside paths to the goal in nearly all conditions. However, as shown in Figure 15C, the distribution of paths shifted systematically across conditions, such that the percentage of inside paths increased with the offset angle and the nearness of the goal. On average, participants switched from an outside path to an inside path at an offset angles between 2° and 4°, and they were more likely to do so when the goal was nearer. A two-way analysis of variance on the percentage of inside paths revealed significant main effects of offset angle, $F(3, 27) = 94.83$, $p < .01$, and goal distance, $F(2, 18) = 53.46$, $p < .01$, with no interaction, $F(6, 54) = 1.17$, $p = .34$. In summary, participants were more likely to switch from an outside to an inside path as offset angle increased and goal distance decreased. This confirms the necessity of including an explicit term for goal distance in the model.

Simulations. We tested the model on scene configurations similar to those in Experiment 3. The initial goal distance varied between 5 and 9 m, and the initial offset angle between 1° and 15°, while the initial goal angle (15°) and initial obstacle distance (4 m) were held constant. Our first set of simulations used parameter values determined from Experiment 1b for the goal component and Experiment 2 for the obstacle component, as before. The model successfully predicts the shift from outside to inside paths with larger offset angles and nearer goals. Specifically, it generates an outside path for offset angles ≤ 7° and an inside path for angles ≥ 10°. Between 7° and 10°, the model takes an outside path with larger goal distances and switches to an inside path with smaller goal distances, replicating the qualitative pattern of human routes.

The shift to inside paths, however, occurred at somewhat larger offset angles for the model (7–10°) than for human participants (2–4°). Thus, using parameter settings based on Experiments 1 and 2, the model is somewhat biased toward outside paths. One reason for this may be that the first two experiments sampled a limited range of conditions, and in particular they did not include cases in which participants crossed in front of the obstacle to reach the goal. It is possible that participants adapted their behavior (adjusted their "parameters") to these conditions, so the parameter fits did not generalize precisely to a wider range of conditions. We thus performed a second set of simulations to determine whether we could reproduce the pattern of routes observed in Experiment 3 with a minimal change in parameter values. Adjusting a single parameter, c_4, from 0.8 to 1.6, was sufficient to induce the shift from an outside to an inside path at offset angles of 1° to 4° (see

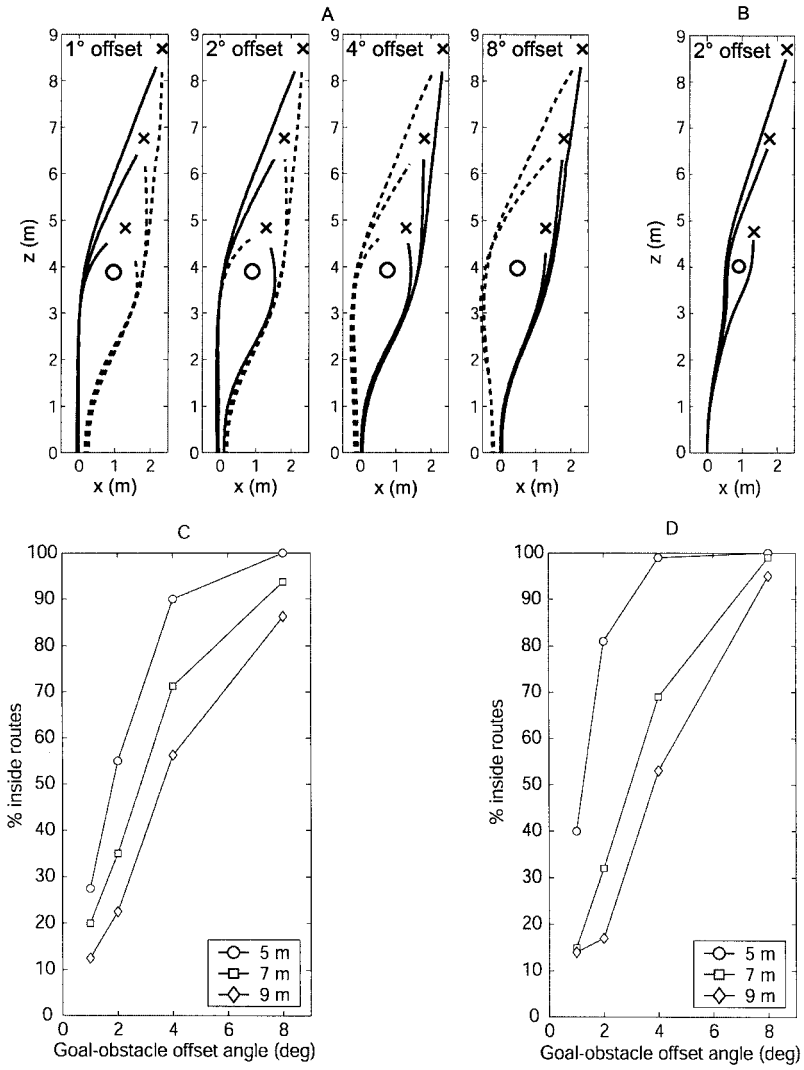

Figure 15. Experiment 3 data. A: Mean paths in the 5-, 7-, and 9-m initial goal distance conditions for each initial goal-obstacle offset angle. Solid lines correspond to the most frequently selected route in each condition. B: Simulated paths with an initial offset angle of 2°, with parameter $c_4 = 1.6$. C: Percentage of inside paths as a function of initial goal-obstacle offset angle for each condition of initial goal distance. D: Model simulations of the percentage of inside paths, with 10% error in perceptual variables and parameters and variability in initial conditions matched to the human data.

Figure 15B). This increased the decay rate of obstacle repulsion with distance, allowing closer approaches to obstacles, and thus c_4 might be thought of as a "risk" parameter.

In these simulations, the effect of initial goal distance is a consequence of the fact that the attractive strength of the goal, and hence angular acceleration toward it, increase for nearer goals. The effect of offset angle is a consequence of the trade-off between the attractive strength of the goal, which increases with angle, and the repulsive strength of the obstacle, which decreases with angle. Initially, the goal component dominates, turning the agent in the direction of the goal. However, the resulting decline in both goal and obstacle angles reduces the attractive strength of the goal while increasing the repulsive strength of the obstacle. Whether the agent follows an inside or outside path depends on which component dominates as the agent heads toward the obstacle. For small offset angles, illustrated in Figure 16A–B, the goal angle is relatively small as the agent turns toward the obstacle. Hence, obstacle repulsion overcomes goal attraction, forcing the agent onto an outside path. For large offset angles, in Figure 16C–D, the goal angle is larger as the agent turns toward the obstacle. Hence, goal attraction overcomes obstacle repulsion, drawing the agent onto an inside path. Thus, the observed route arises from competition between goal attraction and obstacle repulsion in the behavioral dynamics.

Model dynamics. To gain a better understanding of the underlying dynamics, we plotted vector fields at several positions on typical inside and outside routes (see Figure 17). Each plot represents the state space of heading (ϕ) by turning rate ($\dot{\phi}$) for one

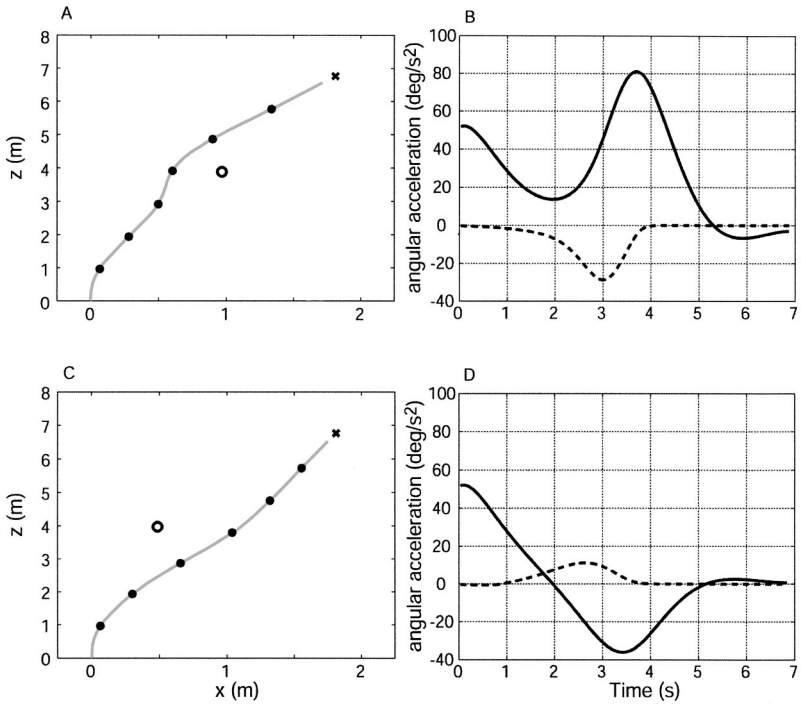

Figure 16. Plots of changing contributions of goal and obstacle components for a sample outside route with a 1° offset angle (A, B) and inside route with an 8° offset angle (C, D). In A and C, black circles along paths represent 1-s time intervals, and black crosses represent the goal. In B and D, solid lines correspond to goal component, and dotted lines correspond to obstacle component. Positive acceleration is in the clockwise direction, and negative acceleration is in the counterclockwise direction.

position in the environment. The small vectors illustrate the flow of the system at each point in state space, the horizontal component corresponding to the change in X (angular velocity $\dot{\phi}$) and the vertical component corresponding to the change in Y (angular acceleration $\ddot{\phi}$) at that point. The heavy line is the *nullcline* at which acceleration is zero and the vectors are purely horizontal. Its intersections with the X-axis (the other nullcline, at which velocity is zero) identify the system's fixed points.

Because the four-dimensional system is difficult to visualize (i.e., ϕ, $\dot{\phi}$, x, and z), we plot vector fields for a sequence of (x, z) positions to better understand how the dynamics change as the agent moves through this four-dimensional space. In Figure 17A, the goal is initially located at 15° and 7 m and the obstacle at 11° and 4 m from the agent's starting position at (x, z) = (0, 0). In the corresponding vector field (Figure 17B), there is a single attractor at (ϕ, $\dot{\phi}$) = (15.2°, 0°/s), near the goal direction of ψ_g = 15.0° (filled arrow) on the other side from the obstacle (open arrow). Although the location of the attractor is determined by the combination of the goal and obstacle components, the goal component dominates at this point because the goal angle is large and the obstacle is distant, so the attractor is located near the goal direction.

In Figure 17C, when the agent is to the left of the obstacle at (x, z) = (0.4, 3.2), the goal and obstacle components interact considerably. The system is bistable, with attractors at (2.8°, 0°/s) and (46.3°, 0°/s), separated by a saddle point at (27.1°, 0°/s). The form of this shift from one- to two-point attractors is analogous to a *tangent bifurcation* in a first-order system (Strogatz, 1994). The bistability means that the agent may accelerate either to the left or right of ψ_g = 21.6°, depending on the current heading and turning rate. Note that although the two attractors lie to the left and right of the obstacle at ψ_o = 26.6°, they do not necessarily yield outside and inside paths, respectively. Because the vector field changes as the agent's (x, z) position changes, the location and number of attractors change as well.

In Figure 17D, the agent is passing to the right of the obstacle at (x, z) = (1, 3) and there is a single attractor at (19.2°, 0°/s). The attractor is located slightly to the right of the goal at ψ_g = 12.2° because the obstacle at ψ_o = −14.3° still exerts an influence, pushing the agent slightly to the right of the goal and well away from the obstacle. After the agent is past the obstacle at (x, z) = (1.25, 5.0) in Figure 17E, the obstacle exerts no influence and there is a single attractor at (24.0°, 0°/s), in the same direction as the goal at ψ_g = 24.0°. Thus, the attractor locations are determined by the competition between goal and obstacle components. Where the obstacle component is weak, there is only a single attractor near the goal direction. Where the obstacle component is strong, more than one attractor may exist and none is aligned with the goal. In this way the attractor landscape evolves as the agent moves through the environment, and its behavior is structured by both attractors and repellers.

Perceptual and parameter error. It is apparent from Figure 15 that there was some variation in human routes that is not reproduced by the model, as indicated by the distribution of paths on

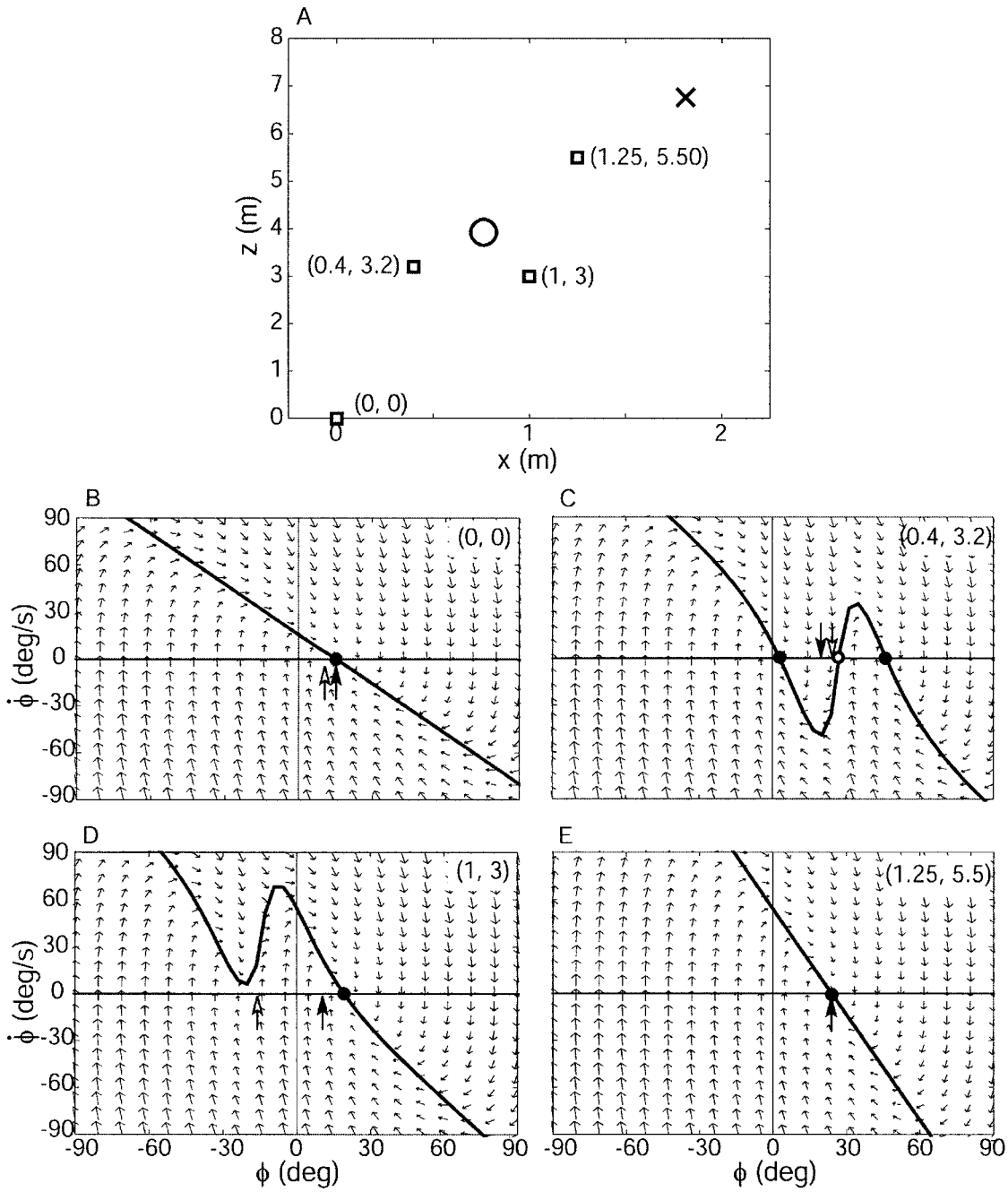

Figure 17. A: Vector fields (ϕ vs. $\dot{\phi}$) at four points along typical outside and inside routes. B–E: For small vectors, the vertical component represents angular acceleration ($\ddot{\phi}$), and the horizontal component represents angular velocity ($\dot{\phi}$). Solid curves represent nullclines at which $\ddot{\phi}$ is zero. Filled circles represent point attractors, and empty circles represent repellers. Filled arrows indicate the goal direction (ψ_g), and open arrows indicate the obstacle direction (ψ_o).

either side of the obstacle. This might be captured by the introduction of variable error in perceptual variables (i.e., goal and obstacle angle and distance) and parameters. At the same time, it is important to determine whether the model is reasonably robust to such error. We investigated the robustness issue by adding variability to each perceptual variable and each parameter, both individually and in various combinations, for selected configurations used in Experiments 1 and 2. On each simulated trial, an error constant was randomly selected for each perceptual variable or parameter from a Gaussian distribution with a mean of 1.0 and a standard deviation of 0.1. Variable error was added to the model by multiplying the actual value of each perceptual variable or

parameter by the corresponding error constant. For the Experiment 1 configuration, initial goal angle was 20° and initial goal distance was 4 m. For the Experiment 2 configuration, initial obstacle angle was −4° and initial obstacle distance was 4 m. The effect of error was measured by taking the standard deviation of the *x*-coordinate halfway through the trial (Experiment 1 configuration) or when the *z*-coordinate equaled that of the obstacle (Experiment 2 configuration). The results, based on 1,000 simulations for each perceptual variable or parameter (or combination), using 10% error are summarized in Table 2. Parameter error yielded slightly more variability than perceptual error, but in all cases the model tolerated both types of error quite well. Even when 10% error was added to all perceptual variables and parameters at the same time, the standard deviation of *x*-position was only 4.15 cm in the Experiment 1 configuration and 11.55 cm in the Experiment 2 configuration.

We then determined whether the distribution of human paths observed in Experiment 3 could be reproduced by introducing variable error. We simulated the model under the same conditions used in Experiment 3, adding 10% error to each perceptual variable and parameter. We also randomly varied the initial *x*-position and heading on each simulated trial, matching the standard deviation to the mean standard deviation observed in Experiment 3 ($SD = 0.16$ cm for initial *x*-position and $SD = 6.58°$ for initial heading). The percentage of inside paths is plotted as a function of initial offset angle for each initial goal distance in Figure 15D. Comparing the simulations to the human data in Figure 15C, it is clear that the observed distribution of paths can be effectively reproduced by adding variable error to the model and matching the initial conditions.

Thus, the model can predict the qualitative behavior of human route selection using parameter settings from Experiments 1 and 2, and it can reproduce those routes quantitatively with an adjustment in a single "risk" parameter. Furthermore, the distribution of human paths is captured by the addition of 10% perceptual and parameter error in the model and variation in initial conditions. This pattern of results demonstrates that simple route selection can be accounted for in terms of elementary behavioral components for steering and obstacle avoidance.

Table 2
Effects of 10% Perceptual and Parameter Errors in Experiment 1 and 2 Configurations

	SD of *x*-position	
Source of error	Experiment 1	Experiment 2
Perceptual variables		
Goal angle	1.51	1.26
Goal distance	1.78	1.21
Obstacle angle		4.39
Obstacle distance		3.82
All	2.06	6.63
Parameters		
b	2.52	2.56
k_g	2.79	2.90
c_1	1.74	1.17
c_2	1.98	2.41
k_o		2.39
c_3		6.89
c_4		4.13
All	4.05	9.44
Perceptual variables and parameters		
All	4.15	11.55

General Discussion

In the research we report here, we sought to derive a model of the behavioral dynamics of human steering and obstacle avoidance and use it to predict route selection in simple scenes. In the first experiment, we collected descriptive data on walking toward a goal and found that steering exhibited point attractor dynamics that depended on initial goal angle and distance. In the second experiment, similar data on obstacle avoidance revealed repeller dynamics that also depended on initial obstacle angle and distance. We modeled the steering dynamics as a linear combination of a goal term and an obstacle term. The attraction of the goal increased linearly with its angle from the current heading and decreased exponentially with distance, whereas the repulsion of the obstacle decreased exponentially with angle and with distance. In the last experiment, we used the model to predict route selection in the simplest case of steering to the left or right of an obstacle. Parameter settings derived from the first two experiments generated the qualitative pattern of routes, and an adjustment in one "risk" parameter reproduced them quantitatively. Steering behavior, obstacle avoidance, and route selection thus emerge from a system that simply follows locally specified attractors.

We believe the contributions of this work are threefold. First, the results provide the first parametric data of which we are aware on the fundamental human behavior of walking to goals and avoiding obstacles. Second, the model represents the extension of a dynamical systems analysis from simple laboratory tasks with stationary dynamics to complex behavior whose dynamics depend on the interaction between the agent and the environment. Third, the results provide the first demonstration we know of that not only attractors but also repellers serve to structure behavior in biological systems, analogous to the work of Schöner et al. (1995) in robotics.

Regarding the human data, several basic observations can be made. First, people make gradual turns during walking, changing their heading direction over several steps rather than pivoting on one foot to abruptly switch directions, thereby mitigating the inertial effects of changing direction. On the other hand, they do not travel on a continuous arc to the goal, but turn onto an approximately linear path that aligns their heading direction with the goal. This is consistent with the idea that, at least in open field walking, people control their current heading so that it is aligned with the goal, and it is contrary to theories that suggest people follow curved paths to a target (Lee, 1998; Wann & Swapp, 2000). Second, the rate of turning is influenced by both the distance of a goal or obstacle and its angle with respect to the heading direction. Turning is thus not a biomechanically stereotyped act but appears to be governed by information about the observer's movement relative to objects in the scene.

Dynamics of Steering and Obstacle Avoidance

The model itself can be evaluated in two ways: as a descriptive model of the behavioral dynamics of steering and obstacle avoidance and as a predictive model of route selection. In the first instance, we believe the model does a good job of capturing the behavioral dynamics. It compactly describes the behavior of steering toward a goal or around an obstacle with fits near $r^2 = 1.0$. The linear combination or superposition of goal and obstacle terms is advantageous because the model scales linearly with the complexity of the scene, adding a term for each new object (Large, Christensen, & Bajcsy, 1999). In practice, the model is even more efficient, because it only depends on information about objects that appear within a restricted zone in depth and about the current heading. Specifically, the obstacle component decreases to near zero at a distance of about 4 m and an angle of $\pm 60°$ from the heading direction (Figure 2B). This implies that human steering behavior is not based on the complete 3-D layout of the scene, but on a limited sample of the next few objects near the path of travel. Such a result is consistent with use of on-line information for steering control, rendering a detailed internal world model and explicit path planning unnecessary.

Another type of internal representation often thought to be necessary for control is a model of the *plant dynamics* (Loomis & Beall, 1998). Such a model of the relationship between control variables and resulting body movements would allow the agent to predict future states of the body. However, if behavior is a consequence of laws of control and physical constraints, an explicit model of the plant dynamics is unnecessary. Instead, the agent might simply learn parameter settings for the control law that yield successful behavior within the given physical constraints. If these constraints change (e.g., if the agent's mass increases or the medium changes from air to water), the agent may adapt by tuning the parameters to stabilize behavior again. Thus, the agent's "model" of the plant dynamics is simply a set of parameter values that result in successful behavior within given constraints.

Route Selection

We also believe that the model is a promising first account of route selection. By fitting the model to human data from the limited conditions of Experiments 1b and 2, we were able to predict the qualitative pattern of routes observed in the simple case in Experiment 3. It is likely that fitting the model to data from more general conditions would allow us to make more quantitative predictions. Thus, our current research fixes parameters on the basis of Experiment 3 and attempts to predict human routes through more complex scenes by linearly combining terms for goals and obstacles, including pairs of obstacles, random arrays of obstacles, and cul-de-sacs (Fajen, Beem, & Warren, 2002).

The main limitation of the model is that it currently represents obstacles as points. This is unrealistic for complex scenes that contain wide obstacles or extended surfaces such as walls. Such objects might be represented in the model either by adjusting the decay rate of the repulsion function (parameter c_3 in Equation 12; see Figure 2B), or by treating a wide obstacle as a set of points at finite intervals and summing their influence. The latter predicts that people turn away from wide obstacles faster than from small ones. The effects of obstacle width on steering behavior and route selection remain to be empirically investigated. On the other hand, body width is implicitly represented in the model by the "risk" parameter c_4, the decay rate of repulsion with distance (Warren & Whang, 1987).

A next step is to generalize the model from stationary goals and obstacles to moving goals and obstacles. In recent experiments, we found that humans intercept moving targets by seeking to achieve a constant angle between the target and the heading (Fajen & Warren, 2002). This can be incorporated in the model by adding a term to the goal angle that depends on the angular velocity of the target ($\dot{\psi}_g$), so as to shift the attractor ahead of the target by an amount proportional to target speed. A similar term might be inserted into the obstacle component to avoid moving obstacles. When the steering model for an individual agent is complete, it would allow us to simulate the behavior of multiple interacting agents in a dynamic environment, including crowd behavior.

The present results demonstrate that it is possible, in principle, to account for human route selection as a consequence of elementary behaviors for steering and obstacle avoidance. In effect, the agent adopts a particular route through the scene on the basis of local responses to visually specified goals and obstacles. The observed route is not determined in advance through explicit planning, but rather emerges in an on-line manner from the agent's interactions with the environment. It is possible, of course, to develop an off-line path planning account of the results from Experiment 3; the model simply demonstrates that a more parsimonious on-line account is plausible and adequate to the data. It is also possible that familiarity with the layout of goals and obstacles would influence route selection in a manner that cannot be captured by the model in its current form. We are currently investigating how route selection changes with experience and considering ways of expanding the model to accommodate these changes. Such changes might simply be captured by the tuning of parameters in the model.

Behavioral Dynamics and Control Laws

The present model differs from the robotic control model of Schöner et al. (1995) in two closely related ways. First, because it describes the observed behavior of an inertial agent, we were forced to abandon a first-order system and adopt a higher-order system. Second, our model treats steering adjustments as transient behavior en route to a stable attractor (heading in the goal direction). In contrast, Schöner et al.'s model is a first-order system that is at all times in an attractor state and thus stable at every moment. The significance of such a first-order model is that it permits the integration of multiple constraints (goals and obstacles in arbitrary positions) in such a way that a solution can be assured, guaranteeing that the observer does not collide with an obstacle, become trapped in a local minimum, oscillate between two goals, or not reach the goal. In contrast, there is no way to ensure that transient solutions satisfy multiple arbitrary constraints. These differences follow directly from Schöner et al.'s modeling of a control system at the first level of analysis, whereas we modeled the behavioral dynamics of a physical agent at the second level of analysis. First-order control laws may be advantageous to achieve well-behaved solutions under multiple constraints. At the same time, observed behavior is a consequence of these control laws interacting with the physics of the body and environment and thus requires

a higher-order description. As outlined in the introduction, we suggest that these two levels of analysis, and hence the two models, are complementary. Now that we have a formal description of the behavioral dynamics of steering, we can consider whether a first-order control law can give rise to this behavior.

Let us assume that a first-order control law is embedded within a second-order system representing the physical body. The form of the control law can be borrowed from the terms in our model, which capture the behavioral influence of goals and obstacles:

$$\dot{\phi}' = -k_g(\phi - \psi_g)(e^{-c_1 d_g} + c_2) + k_o(\phi - \psi_o) \times (e^{-c_3|\phi-\psi_o|})(e^{-c_4 d_o}). \quad (13)$$

This control law is a dynamical system that takes the visually specified current heading, goal angle and distance, and obstacle angles and distances, and immediately relaxes to an attractor for the intended heading at a value ϕ^*. A prime has been added to the angular acceleration ($\ddot{\phi}'$) to distinguish the control law from physical acceleration of the body. Note that ϕ^* is determined by the combination of goal and obstacle terms, and it may not necessarily correspond to the direction of the goal. Given the intended heading, the angular acceleration of the body is then determined by a second-order system, whose parameters are independent of the layout of goals and obstacles in the world:

$$\ddot{\phi} = -b_b\dot{\phi} - k_b(\phi - \phi^*). \quad (14)$$

Because of the body's inertia, the resulting behavior has a slower relaxation time than the control law, so the actual heading lags behind the intended heading. Thus, whereas the control law tracks a stable attractor, the observed behavior is transient. Note that this concept of a control law as a dynamical system is distinct from conceiving of it as a simple mapping from an optical variable to an action variable.

In simulations performed by Philip Fink (a postdoctoral research associate in the VENLab), we tested this embedded model with a goal and one obstacle, under the conditions of Experiment 2. Mean paths were nearly identical to those of the higher order model, and least-squares fits to the mean time series of goal angle had a mean $r^2 = .991$. The resulting parameter values, which were naturally different from the higher order model, were $k_g = 59.1625$, $c_1 = 0.0555$, $c_2 = 0.01125$, $k_o = 842$, $c_3 = 2.74063$, $c_4 = 0.04653$, $b_b = .0375$, and $k_b = 592$. Thus, the higher order behavioral dynamics that we observed experimentally can be accounted for in terms of a first-order control system, preserving the advantages of a stable solution that satisfies multiple constraints. These results demonstrate that the behavior of steering and obstacle avoidance can be modeled consistently at two levels, the first involving interactions between a first-order control law and the physics of the body and world, and the second providing a higher order description of the emergent behavior.

It is important to show that the informational variables in the control law are perceptually available. Although we parameterized the model in terms of object distance, the control law might be based on either the perceived distance of the object or the perceived time-to-contact specified by the optical τ variable (Bootsma & Craig, 2002; Lee, 1980). Given that the influence of obstacles gradually asymptotes to zero around 4 m and the influence of the goal to a constant value beyond 8 m, accurate perception of distance or time-to-contact is not essential. With time-to-contact less than 4 s, obstacles are within the range of sensitivity to τ (Schiff & Detwiler, 1979), and given that the control process is continuous accuracy improves as an obstacle is approached.

Goal and obstacle angles are also perceptually specified. Warren et al. (2001) found that walking is guided by a combination of the visual direction of the goal with respect to the heading specified by optic flow ($\phi_{flow} - \psi_g$), and the egocentric direction of the goal with respect to the locomotor axis, which is presumably specified proprioceptively ($\phi_{loco} - \psi_g$). Thus, we can expand the informational term in the goal component of the control law as

$$\phi - \psi_g = (\phi_{loco} - \psi_g) + wv(\phi_{flow} - \psi_g), \quad (15)$$

where v is observer velocity and w represents environmental structure, both of which influence the magnitude and area of optic flow. It remains to be empirically determined whether the obstacle component can be similarly expanded.

Comparison With Other Models

Our dynamical model bears a resemblance to potential field models of path planning (Khatib, 1986), which also represent behavior as transients to attractor states. However, in comparative simulations of the two models, we observed some notable differences (see Fajen, Warren, Temizer, & Kaelbling, in press, for details). First, in the potential field approach the attractors and repellers are defined as the two-dimensional positions of goals and obstacles in the world, whereas the dynamical approach defines them as values of the behavioral variables (heading and turning rate). Thus, whereas behavior is determined by the agent's position in the potential field model, behavior in our dynamical model is determined by the agent's position, heading, and turning rate. Second, whereas potential field models control translation direction, the present dynamical model determines angular acceleration and thus tends to yield smoother trajectories. Third, as a consequence of acceleration, our dynamical model can produce different paths for different translation speeds. In contrast, because the potential field equations determine the direction of the agent's motion from its position, it always traverses the same path regardless of speed. Finally, comparative simulations reveal that the dynamical model generates markedly smoother and shorter paths to the goal and that local minima can be avoided by reducing the decay rate of the "risk" parameter c_4.

We should point out that the observed human paths depart dramatically from a simple shortest path criterion (see particularly Figure 15). To our knowledge, no other models have been proposed for locomotor paths that take obstacle avoidance into account. Note that the present model does not incorporate an explicit optimality principle, although its form or parameter values could result from such principles over the course of evolution or learning, such as a combination of minimizing energy and injury.

Conclusion

In summary, the present model captures the behavioral dynamics of human steering and obstacle avoidance with good fidelity, and it can reproduce the pattern of routes through a simple scene. This suggests that human route selection does not require explicit planning but may emerge on-line as a consequence of elementary

behaviors for steering and obstacle avoidance. We are currently investigating whether the present form of the model can also account for route selection in more complex scenes.

References

Bootsma, R. J., & Craig, C. M. (2002). Global and local contributions to the optical specification of time to contact: Observer sensitivity and composite tau. *Perception, 31,* 901–924.

Brooks, R. A. (1991). Intelligence without representation. *Artificial Intelligence, 47,* 139–160.

Collins, J. J., & Stewart, I. (1993). Hexapodal gaits and coupled nonlinear oscillator models. *Biological Cybernetics, 68,* 287–298.

Diedrich, F. J., & Warren, W. H. (1995). Why change gaits? Dynamics of the walk-run transition. *Journal of Experimental Psychology: Human Perception and Performance, 21,* 183–202.

Duchon, A. P., & Warren, W. H. (2002). A visual equalization strategy for locomotor control: Of honeybees, robots, and humans. *Psychological Science, 13,* 272–278.

Duchon, A. P., Warren, W. H., & Kaelbling, L. P. (1998). Ecological robotics. *Adaptive Behavior, 6,* 473–507.

Fajen, B. R. (2001). Steering toward a goal by equalizing taus. *Journal of Experimental Psychology: Human Perception and Performance, 27,* 953–968.

Fajen, B. R., Beem, N., & Warren, W. H. (2002, May). *Route selection emerges from the dynamics of steering and obstacle avoidance.* Paper presented at the 2nd Annual Conference of the Vision Sciences Society, Sarasota, FL.

Fajen, B. R., & Warren, W. H. (2002). *Intercepting a moving target on foot.* Manuscript submitted for publication.

Fajen, B. R., Warren, W. H., Temizer, S., & Kaelbling, L. P. (in press). A dynamical model of visually-guided steering, obstacle avoidance, and route selection. *International Journal of Computer Vision.*

Gibson, J. J. (1979). *The ecological approach to visual perception.* Boston: Houghton Mifflin.

Gibson, J. J. (1998). Visually controlled locomotion and visual orientation in animals. *Ecological Psychology, 10,* 161–176. (Reprinted from *British Journal of Psychology, 49,* 182–194, 1958)

Jeka, J. J., Kelso, J. A. S., & Kiemel, T. (1993). Spontaneous transitions and symmetry: Pattern dynamics in human four-limb coordination. *Human Movement Science, 12,* 627–651.

Kay, B. A., & Warren, W. H. (2001). Coupling of posture and gait: Mode locking and parametric excitation. *Biological Cybernetics, 85,* 89–106.

Kelso, J. A. S. (1995). *Dynamic patterns: The self-organization of brain and behavior.* Cambridge, MA: MIT Press.

Khatib, O. (1986). Real-time obstacle avoidance for manipulators and mobile robots. *International Journal of Robotics Research, 5,* 90–98.

Kugler, P. N., & Turvey, M. T. (1987). *Information, natural law, and the self-assembly of rhythmic movement.* Hillsdale, NJ: Erlbaum.

Land, M. (1998). The visual control of steering. In L. R. Harris & H. Jenkins (Eds.), *Vision and action* (pp. 163–180). New York: Cambridge University Press.

Large, E. W., Christensen, H. I., & Bajcsy, R. (1999). Scaling the dynamic approach to path planning and control: Competition among behavioral constraints. *International Journal of Robotics Research, 18,* 37–58.

Lee, D. N. (1980). Visuo-motor coordination in space-time. In G. E. Stelmach & J. Requin (Eds.), *Tutorials in motor behavior* (pp. 281–295). Amsterdam: North-Holland.

Lee, D. N. (1998). Guiding movement by coupling taus. *Ecological Psychology, 10,* 221–250.

Li, L., & Warren, W. H. (2002). Retinal flow is sufficient for steering during simulated rotation. *Psychological Science, 13,* 485–491.

Loomis, J. M., & Beall, A. C. (1998). Visually controlled locomotion: Its dependence on optic flow, 3-D space perception, and cognition. *Ecological Psychology, 10,* 271–285.

Meyer, J. A., & Wilson, S. W. (Eds.). (1991). *From animals to animats.* Cambridge, MA: MIT Press.

Moravec, H. P. (1981, August). *Obstacle avoidance and navigation in the real world by a seeing robot rover.* Proceedings of the 7th International Joint Conference on Artificial Intelligence, Los Altos, CA.

Reichardt, W., & Poggio, T. (1976). Visual control of orientation behavior in the fly: I. A quantitative analysis. *Quarterly Review of Biophysics, 9,* 311–375.

Rushton, S. K., Harris, J. M., Lloyd, M., & Wann, J. P. (1998). Guidance of locomotion on foot uses perceived target location rather than optic flow. *Current Biology, 8,* 1191–1194.

Schiff, W., & Detwiler, M. L. (1979). Information used in judging impending collision. *Perception, 8,* 647–658.

Schöner, G., & Dose, M. (1992). A dynamical systems approach to task-level system integration used to plan and control autonomous vehicle motion. *Robotics and Autonomous Systems, 10,* 253–267.

Schöner, G., Dose, M., & Engels, C. (1995). Dynamics of behavior: Theory and applications for autonomous robot architectures. *Robotics and Autonomous Systems, 16,* 213–245.

Schöner, G., Jiang, W. Y., & Kelso, J. A. S. (1990). A synergetic theory of quadrupedal gaits and gait transitions. *Journal of Theoretical Biology, 142,* 359–391.

Strogatz, S. H. (1994). *Nonlinear dynamics and chaos.* Reading, MA: Addison-Wesley.

Wann, J. P., & Swapp, D. K. (2000). Why you should look where you are going. *Nature Neuroscience, 3,* 647–648.

Warren, W. H. (1988). Action modes and laws of control for the visual guidance of action. In O. Meijer & K. Roth (Eds.), *Movement behavior: The motor-action controversy* (pp. 339–380). Amsterdam: North-Holland.

Warren, W. H. (1998). Visually controlled locomotion: 40 years later. *Ecological Psychology, 10,* 177–219.

Warren, W. H. (2002). *The dynamics of perception and action.* Unpublished manuscript.

Warren, W. H. (in press). Optic flow. In L. Chalupa & J. S. Werner (Eds.), *The visual neurosciences.* Cambridge, MA: MIT Press.

Warren, W. H., Kay, B. A., Zosh, W. D., Duchon, A. P., & Sahuc, S. (2001). Optic flow is used to control human walking. *Nature Neuroscience, 4,* 213–216.

Warren, W. H., & Whang, S. (1987). Visual guidance of walking through apertures: Body scaled information for affordances. *Journal of Experimental Psychology: Human Perception and Performance, 13,* 371–383.

(*Appendix follows*)

Appendix

Full Model Equations

The full model is given by the following equation:

$$\ddot{\phi} = -b\dot{\phi} - k_g(\phi - \psi_g)(e^{-c_1 d_g} + c_2) + \sum_{i=1}^{\#obstacles} k_o(\phi - \psi_{o_i})\, e^{-c_3|\phi - \psi_{o_i}|}(e^{-c_4 d_{o_i}}). \quad \text{(A1)}$$

Note that ψ_g, d_g, ψ_o, and d_o change as the position of the agent changes (see Figure 1A). However, each of these variables can be expressed as a function of the (x, z) position of the observer:

$$\psi_g = \cos^{-1}\left[\frac{(Z_g - z)}{d_g}\right], \quad \text{(A2)}$$

$$d_g = [(X_g - x)^2 + (Z_g - z)^2]^{1/2}, \quad \text{(A3)}$$

$$\psi_o = \cos^{-1}\left[\frac{(Z_o - z)}{d_o}\right], \quad \text{(A4)}$$

and

$$d_o = [(X_o - x)^2 + (Z_o - z)^2]^{1/2}, \quad \text{(A5)}$$

where (X_g, Z_g) and (X_o, Z_o) are the coordinates of the goal and obstacle, respectively. Written as a system of first-order differential equations, the model is given by the following:

$$\dot{y}_1 = \dot{\phi},$$

$$\dot{y}_2 = \ddot{y}_1 = \ddot{\phi} = -by_2 - k_g(y_1 - \psi_g)(e^{-c_1 d_g} + c_2) + \sum_{i=1}^{\#obstacles} k_o(y_1 - \psi_{o_i})\, e^{-c_3|y_1 - \psi_{o_i}|}(e^{-c_4 d_{o_i}}), \quad \text{(A6)}$$

$$\dot{y}_3 = \dot{x} = V \sin y_1,$$

$$\dot{y}_4 = \dot{z} = V \cos y_1,$$

where V is the speed of the observer, which was held constant at 1 m/s in our simulations.

Received August 3, 2001
Revision received May 24, 2002
Accepted August 27, 2002 ■